Implications of different nitrogen input sources for potential production and carbon flux estimates in the coastal Gulf of Mexico (GOM) and Korean coastal waters

Jongsun Kim [a*] Piers Chapman [a, c], Gilbert Rowe [a, b], Steven F DiMarco [a, c], and Daniel C. O. Thornton[a]

[a] Department of Oceanography, Texas A&M University, College Station, TX 77843-3146, USA

[b] Department of Marine Biology, Texas A&M University, Galveston, TX 77553, USA

[c] Geochemical and Environmental Research Group, Texas A&M University, College Station, TX 77843-3149, USA

[*] Corresponding author

*J. Kim. Email: jongsun@tamu.edu

Submit to Ocean Sciences

Abstract

The coastal Gulf of Mexico (GOM) and coastal sea off Korea (CSK) both suffer from human-induced eutrophication. We used a nitrogen (N) mass balance model in two different regions with different nitrogen input sources to estimate organic carbon fluxes and predict future carbon fluxes under different model scenarios. The coastal GOM receives nitrogen predominantly from the Mississippi and Atchafalaya Rivers and atmospheric nitrogen deposition is only a minor component in this region. In the CSK, groundwater and atmospheric nitrogen deposition are more important controlling factors. Our model includes the fluxes of nitrogen to the ocean from the atmosphere, groundwater, and rivers, based on observational and literature data, and identifies three zones (brown, green and blue waters) in the coastal GOM and CSK with different productivity and carbon fluxes. Based on our model results, the potential primary production rate in the inner (brown water) zone are over 2 gC m^{-2} day^{-1} (GOM) and 1.5 gC m^{-2} day^{-1} (CSK). In the middle (green water) zone, potential production is between 0.1 to 2 (GOM) and 0.3 to 1.5 gC m^{-2} day^{-1} (CSK). In the offshore (blue water) zone, productivity is less than 0.1 (GOM) and 0.3 (CSK) gC m^{-2} day^{-1}. Through our model scenario results, overall oxygen demand in the GOM would increase approximately 21% if we fail to reduce riverine N input, likely increasing considerably the area affected by hypoxia. Comparing the results from the U.S. with those from Korea shows the importance of considering both riverine and atmospheric inputs of nitrogen. This has direct implications for investigating how changes in energy technologies can lead to changes in the production of various atmospheric contaminants that affect air quality, climate and the health of local populations.

Keywords:

Chemical tracers, Biological processes, Shelf-seas, Gulf of Mexico, Yellow Sea.

Introduction

Industrial expansion and anthropogenic emissions are major factors leading to increased coastal productivity and potential eutrophication (Sigman and Hain 2012). Coastal primary production is controlled largely by nitrogen (N) and phosphorus (P), and the relative supply of each determines which element limits production (Paerl 2009); freshwater inputs and the distance from sources such as river mouths are also important (Dodds and Smith 2016). Changes in nutrient loading from air-borne, river-borne and groundwater sources can also affect which element limits coastal productivity (Sigman and Hain 2012). Most coastal regions are N-limited, however, at certain times conditions can change from N-limited to P-limited (Dodds and Smith 2016; Howarth and Marino 2006). Sylvan et al. (2006), for example, suggested that the coastal GOM, especially near the Mississippi River delta mouth, is P-limited at certain times.

Several studies have shown that increasing atmospheric nitrogen deposition (AN-D) is contributing to ocean production globally, including to eutrophication, and is potentially of future importance in the GOM (Cornell et al., 1995; Doney et al., 2007; Duce et al., 2008; He et al., 2010; Kanakidou et al., 2016; Kim 2018; Kim (TW) et al., 2011; Lawrence et al., 2000; Paerl et al., 2002). Recently, Kim (TW) et al. (2011), using a model simulation showed that AN-D controls approximately 52% of the coastal productivity in the Yellow Sea. Global NOx emissions have increased but appear to be changing differently in the US and Asia (Kim (JY) et al., 2010; Luo et al., 2014; Shou et al., 2018; Zhao et al., 2015), and may affect not only coastal productivity but also global total nitrogen budgets. This study uses a box model to define potential carbon fluxes based on different nitrogen input sources in two different regions, the Coastal Gulf of Mexico (GOM) and the Coastal Sea off Korea (CSK). The GOM and CSK were selected in this study because while the major input source to the coastal ocean in both

regions is riverine, the AN-D and submarine groundwater discharge (SGD) are considerably more important in the CSK region (Wade and Sweet, 2008; Zhao et al., 2015).

Most previous model studies in the GOM have been used to predict the size of the hypoxic zone (e.g., Fennel et al., 2006, 2011, 2013; Green et al., 2008; Hetland and DiMarco 2008; Justic et al., 2002; Scavia et al., 2004; Turner et al. 2006, 2008), although Bierman et al. (1994), used a mass balance model to estimate carbon flux and oxygen exchange. The mass balance model is a useful tool to calculate nutrient or carbon fluxes and to estimate production in the coastal ocean (Kim (JS) et al, 2010; Kim (G) et al., 2011), and such models have been successfully used in many regions and individual coastal systems to estimate ecosystem metabolism, e.g., in the Patuxent River estuary of the Chesapeake Bay (Hagy et al. 2000; Testa et al., 2008) and in the LOICZ (Land Ocean Interactions in the Coastal Zone) project (e.g., Ramesh et al., 2015). However, there are few such model studies in the GOM and CSK. All previous models for the GOM and the CSK have considered only riverine N as the predominant input source, and no one has considered AN-D as an input in either region.

In this study, we aimed to: 1) build a mass balance model considering not only riverine N input but also air-borne and groundwater-borne N; 2) use it to calculate potential primary production in the three regions defined by Rowe and Chapman (2002, henceforth RC02, see next section) and their associated coastal productivity; and 3) use the mass balance model to test the RC02 hypothesis. Because RC02 did not quantify their model with nutrient data and no one has applied this model to another region, we tested the RC02 hypothesis using data from both the GOM and the CSK that include low salinity samples. We used historical data from the mid-western part of the CSK and evaluated the theoretical model of RC02 in both areas where freshwater with high terrestrial nutrient input mixes into the coastal ocean.

47

48 **Study areas**

49 The Texas-Louisiana (LATEX) shelf in the northern Gulf of Mexico is affected by
50 coastal nutrient loading, leading to hypoxia, coming from two major terrestrial sources (the
51 Mississippi and Atchafalaya Rivers that together form the Mississippi-Atchafalaya River System
52 MARS). These two major rivers have different nutrient concentrations. The Gulf of Mexico
53 (GOM) is a semi-enclosed oligotrophic sea and the MARS is the major source of nutrients and
54 freshwater to the northern GOM (Alexander et al., 2008; Rabalais et al., 2002; Robertson and
55 Saad, 2014). The MARS drains 41% of the contiguous United States (Milliman and Meade,
56 1983) and discharges approximately 20,000 m^3 s^{-1}, or about 60% of the total freshwater flow,
57 (about 10.6 x 10^{11} m^3 $year^{-1}$ or 3.4 x 10^4 m^3 s^{-1}) to the northern side of the GOM. The
58 remainder comes from other U.S. rivers, Mexico and Cuba (Nipper et al., 2004).

59 At the Old River Control Structure on the lower Mississippi River approximately 25% of
60 the Mississippi River's water is diverted into the Atchafalaya River, where it mixes with the
61 water in the Red River. The flow in the Atchafalaya River totals 30% of the total MARS flow
62 (Figure 1a). Several projects have investigated the relationship between nutrients and the
63 marine ecosystem, and how this leads to hypoxia in the GOM (e.g. Bianchi et al., 2010; Diaz and
64 Rosenberg, 1995, 2008; Forrest et al., 2011; Hetland and DiMarco, 2008; Laurent et al., 2012;
65 Quigg et al., 2011; Rabalais and Smith, 1995; Rabalais et al., 2007; Rabalais and Turner 2001;
66 Rowe and Chapman 2002). Strong stratification due to the high freshwater discharge from the
67 MARS, local topography (DiMarco et al., 2010), wind direction, and high nitrate concentration
68 all affect hypoxia formation, with upwelling-favorable wind facilitating its development (Feng et
69 al., 2012, 2014).

In the Northern GOM, the major factor controlling coastal productivity is riverine N input. Rowe and Chapman (2002), defined three theoretical zones over the LATEX shelf close to the Mississippi and Atchafalaya River mouths to predict the effects of nutrient loading on hypoxia along the river plumes and over the shelf. They named these the brown, green, and blue zones (Figure 2). Nearest the river mouths is a 'brown' zone, where the nutrient concentrations are high, but the discharge of sediment from the river reduces light penetration and limits primary productivity within the plume. Further away from the river plume is a stratified 'green' zone with available light and nutrients that result in high productivity. In this region, the rapid depletion of nutrients is due to biological uptake processes that depend on the season and river flow (Bode and Dortch, 1996; Dortch and Whitledge, 1992; Lohrenz et al., 1999; Turner and Rabalais, 1994). Still further offshore, and also along the river plume to the west, there is the so-called 'blue' zone, defined arbitrarily by nitrate concentrations of 1 μM or less, which is dominated by intense seasonal stratification and a strong pycnocline, so that in the surface layer nutrients are limiting at this distance from the rivers and most primary production is fueled by recycled nutrients (Dortch and Whitledge, 1992). It is important to note that RC02 makes clear that the edges of the zones (geographical regimes) are not static, but change over time depending on season, river flow, and biological processes (Figure 2).

The coastal sea off western Korea (CSK) forms the eastern side of another semi-enclosed basin (the Yellow Sea) and is affected by freshwater discharge from river plumes in the same way as the coastal GOM, although the freshwater flow is considerably less. The Yellow Sea covers about 380,000 km^2 area with an average water depth of 44 m, and numerous islands are located on its eastern side (Liu et al., 2003). Our specific study area is the mid-western coastal region from the Taean Peninsula to Gomso Bay (Figures 1c and 1d).

There is a strong tidal front in the coastal area near the Taean Peninsula due to sea floor topography and the coastal configuration (Park, 2017; Park et al., 2017). The region also contains several bays (Garolim Bay, Gomso Bay and Cheonsu Bay), and is affected by discharges from a large artificial lake (Saemangeum lake) as well as the freshwater discharge from the Keum river plume that contains high concentrations of nutrients (Lim et al., 2008). Conditions in the mid-western CSK near the Taean peninsula are similar to the coastal GOM, because of mixing of two different water masses from Gyunggi Bay (Han River) and the Keum River (Choi et al., 1998, 1999). The annual mean flow rates within the Keum River were about 70 m^3 s^{-1} (normal period) and 170 m^3 s^{-1} (flood period) (Yang and Ahn 2008). Precipitation within the catchment was 1,208 mm $year^{-1}$ during 2003 to 2005 (Yang and Ahn 2008).

Unlike the coastal GOM, the CSK has increased nitrogen inputs from atmospheric nitrogen deposition (AN-D, which is approximately five times higher than in the GOM, Table 2) (Kim (JY) et al., 2010; Luo et al., 2014; Shou et al., 2018; Zhao et al., 2015) and nutrient inputs from the groundwater discharge (Kim (JS) et al., 2010; Kim (G) et al., 2011). AN-D has increased in the CSK owing to industrial development in China during the last few decades, which has led to increased atmospheric N emission.

Data and Methods

Riverine N data

Hydrographic data from the MCH (Mechanisms Controlling Hypoxia – MCH Atlas) projects in the Gulf of Mexico were collected from the National Oceanographic Data Center (https://www.nodc.noaa.gov) covering the period from 2004 through 2007 (Table 1). We excluded cruises MCH M6 and M7 because the threat of hurricanes led to sampling stations in

different areas from the other cruises. The study sites and sampling areas are shown in Figure 1b. Quality control removed inconsistencies and anomalies in the data (e.g., removing outliers, missing data found by linear interpolation). Hydrographic data from the CSK (nutrients, salinity, oxygen) were collected during several cruises (Table 1 and Figure 1c and 1d), and the data were put through similar QA/QC routines.

Atmospheric Nitrogen Deposition (AN-D) data

AN-D data from around the US are sparse (Table 2). Most US data have been collected along the east coast of the US and the only data in the GOM region were collected near Corpus Christi (~1 g m^{-2} $year^{-1}$; Wade and Sweet, 2008), Considerable AN-D could be expected, however, from the large number of petrochemical and fertilizer plants in southern TX, especially near Houston and along the Mississippi. While there are more data from the Yellow Sea (Kim (JY) et al., 2010; Luo et al., 2014; Shou et al., 2018; Zhao et al., 2015), they are still limited owing to the broad sampling coverage. While AN-D data in the Asian region were up to 14 g m^{-2} $year^{-1}$, data from the eastern side of the US were under 1 g m^{-2} $year^{-1}$, even lower than in the GOM, suggesting there is currently not a large contribution from AN-D to total N loads to the North Atlantic Ocean. The approximate order of magnitude difference in AN-D concentrations between the GOM and the CSK is due to the continuing industrial development in East Asia and the resulting N emissions (Wang et al., 2016; Zhao et al., 2015). Lamarque et al., (2013) reported model results, which covers our study regions, and their model appears to underestimate AN-D at the sampling sites compared with observational data in the GOM (Wade and Sweet, 2008). However, the pattern of AN-D inputs between GOM and CSK from Lamarque et al.,

(2013) shows around five times difference between the two regions, which agrees with our data. Thus, in our model, we used observational data for both regions, as shown in Table 2.

Methodology: N-mass balance model

Our model consists of three sub-regions based on sampling locations during MCH cruises (Figure 3), each of which contains a series of one-quarter degree square boxes, as followed by Belabbassi (2006). The quarter degree boxes in this study were separated into an upper box and a lower box, based on pycnocline depth, as defined by a sharp change in density and coincides generally with a minimum change in oxygen concentration of 22.33 μM. We assume steady state conditions, and estimate potential production, which we count as an estimate of potential carbon flux (Figure 3a). Primary production (PP) above the pycnocline is expected to be higher than below it (Anderson 1969; Sigman and Hain, 2012), which means that the two layers have different production rates. The difference in PP between upper and lower boxes also depends on the freshwater discharge rate, which determines nutrient input to the upper layer, seasonal variability, and transfer processes between the layers. While chlorophyll can be found below the pycnocline (DiMarco and Zimmerle, 2017), the fact that it is typically associated with low oxygen concentrations suggests that the phytoplankton are either inactive or, more likely, producing at a very slow rate.

The N-mass balance box model is modified from previous models to calculate the net removal of dissolved inorganic nitrogen (DIN) inside each box, which represents potential primary production (PPP) (De Boer A.M. et al., 2010; Kim (G) et al., 2011) (Equation 1). In this model, DIN concentration includes ammonium (NH_4^+), nitrate (NO_3^-), and nitrite (NO_2^-).

$$F_{River}^{DIN} + F_{Atmo}^{DIN} + F_{Bott}^{DIN} - F_{Export}^{DIN} - F_{Deni}^{DIN} = F_{Removal}^{DIN} \quad \text{– Eq. 1}$$

where, F_{River}^{DIN}, an input term, is DIN flux from each river discharge and calculated with C_{Box}^{DIN}, the DIN concentration in each box, A_{Bott}, the bottom area of each quarter degree box, and F_{River}, river discharge rate ($C_{Box}^{DIN} \times A_{Bott} \times F_{River}$). As another input term, F_{Atmo}^{DIN} is the flux from atmospheric nitrogen deposition. F_{Bott}^{DIN}, the benthic flux is additional input term in the sub-pycnocline layer box. The one quarter degree blue boxes located closest to the Mississippi and Atchafalaya river mouths were assumed to be the only ones affected by riverine input (Figure 3b). As an output term, F_{Export}^{DIN} as an advection term was calculated from the current velocity in each region from observations (Nowlin et al., 1998a, b) and from literature data (Jacob et al., 2000; Lim et al., 2008) and the exchange between boxes from the residence time in each box. Note that water and nutrient exchange can take place through all four sides of each box, so the array is two-dimensional. F_{Export}^{DIN} for water mixing was calculated from these factors; C_{EX}^{DIN} is the difference in DIN concentration between adjacent boxes, V_S is the water volume of each box, and λ_{Mix} is the mixing rate of each box $\left(C_{EX}^{DIN} \times V_S \times \lambda_{Mix}\right)$. We used a reciprocal of the water residence time that we considered to represent horizontal mixing, i.e. dispersion. Another output term is F_{Deni}^{DIN}, denitrification process from the water column, and $F_{Removal}^{DIN}$ is removal by biological production. The details of the model definitions are given below in Table 3 and shown in Figure 3. Each arrow indicates input (blue) and output (red) terms (Figure 3). Input/output terms vary based on whether the boxes are above/below the pycnocline, while there are separate inputs from the Mississippi and Atchafalaya rivers in the GOM and Keum and Han rivers in the CSK, respectively.

183 In order to calculate the net removal of DIN in a box above the pycnocline layer, we used
184 our N-mass balance model in Equation 2.
185
186 $$\boldsymbol{F}_{\boldsymbol{River}}^{\boldsymbol{DIN}} + \boldsymbol{F}_{\boldsymbol{Atmo}}^{\boldsymbol{DIN}} - \boldsymbol{F}_{\boldsymbol{Export}}^{\boldsymbol{DIN}} - \boldsymbol{F}_{\boldsymbol{Sink}}^{\boldsymbol{DIN}} = \boldsymbol{F}_{\boldsymbol{Removal}}^{\boldsymbol{DIN}}$$ – Eq. 2
187
188 The boxes above the pycnocline layer have two input terms: 1) $\boldsymbol{F}_{\boldsymbol{River}}^{\boldsymbol{DIN}}$, riverine N,
189 which affects only a subset of boxes along the edge of each region, and 2) $\boldsymbol{F}_{\boldsymbol{Atmo}}^{\boldsymbol{DIN}}$, atmospheric
190 nitrogen deposition (AN-D), which affects every box equally. The mean value of Asian data, as
191 shown in Table 2 (Kim (JY) et al., 2010; Luo et al., 2014; Shou et al., 2018; Zhao et al., 2015), is
192 used for $\boldsymbol{F}_{\boldsymbol{Atmo}}^{\boldsymbol{DIN}}$ of the CSK region, which is initially five times higher than that of the GOM (1.4
193 X 10^5 mol day^{-1}; Wade and Sweet, 2008). We also considered vertical sinking as an input for
194 the sub-pycnocline layer box and as an output from the upper layer. Other possible input
195 factors might be upwelling/downwelling processes; however, these factors are neglected in the
196 model because both regions are shallow and close inshore (Feng et al., 2014; Lim et al., 2008)
197 and we have no observational data on upwelling/downwelling rates. The output terms are the
198 following: 1) $\boldsymbol{F}_{\boldsymbol{Export}}^{\boldsymbol{DIN}}$, the exchange rate between each box (obtained from the different N
199 concentrations in each box and the mass transfer between them), and 2) $\boldsymbol{F}_{\boldsymbol{Sink}}^{\boldsymbol{DIN}}$, removal by
200 biological production, including sinking (assuming that any other removal factors are neglected
201 above the pycnocline). We tested the RC02 three zone hypothesis in the upper box layer, in
202 which we can also examine the horizontal influence (horizontal extent) of the river plume based
203 on production rates.
204 Below the pycnocline layer we used the revised Equation 3.
205

206 $$F_{Bott}^{DIN} + F_{Sink}^{DIN} - F_{Export}^{DIN} - F_{Deni}^{DIN} = F_{Removal}^{DIN}$$ – Eq. 3

207

208 Equation 3 has two separate input terms; 1) The benthic flux F_{Bott}^{DIN} term contains all the
209 potential input from the bottom sediment (defined here as net DIN release from the bottom
210 sediment) including nutrient regeneration by bacteria, groundwater nutrient inputs, and an uptake
211 of nitrate (NO_3^-) and nitrite (NO_2^-) mainly by sedimentary denitrification (McCarthy et al., 2015;
212 Nunnally et al., 2014), and 2) F_{Sink}^{DIN} term as a vertical sinking from the box above the
213 pycnocline layer, for which we used data from Qureshi (1995). The unit of F_{Sink}^{DIN} was
214 converted to mol day^{-1} from the unit of original data (gN m^{-2} day^{-1}) with area of box (0.25 m x
215 0.25 m) and molar mass of N (14 g mol^{-1}).

216 In the GOM, benthic sediments provide excess ammonium to overlying water by
217 regeneration processes such as remineralization (Lehrter et al., 2012; Nunnally et al., 2014;
218 Rowe et al., 2002). Generally, there is an uptake of nitrate and nitrite mainly by sedimentary
219 denitrification (McCarthy et al., 2015) or dissimilatory nitrate reduction to ammonium (DNRA)
220 and assimilation by benthic microalgae (Christensen et al., 2000; Dalsgaard, 2003; Thornton et
221 al., 2007). Due to this, net DIN flux was used as the value of F_{Bott}^{DIN}, which shows DIN release
222 from bottom sediments to overlying water column. For example, in the GOM, the sum of
223 nitrate and nitrite fluxes to bottom sediments (e.g., May: -10.05, July -61.9, August: -48.42 μmol
224 N m^{-2} h^{-1}) were similar or smaller than the flux of ammonium from bottom sediments (e.g., May:
225 203, July: 152, August: 156 μmol N m^{-2} h^{-1}) off Terrebonne bay (McCarthy et al., 2015). In
226 the CSK, the sum of nitrate and nitrite flux to bottom sediments and ammonium flux are 0.5 ~
227 1.4 mmol N m^{-2} d^{-1} and 1.3 ~ 9.6 mmol N m^{-2} d^{-1}, respectively, which indicated that excess
228 ammonium with additional nitrate and nitrite were released from sediments in this region (Lee et

al., 2012). The release of nitrate and nitrite in the CSK unlike the GOM can be estimated due to high inputs of nitrogen by groundwater in the CSK (Kim (G) et al., 2011) even though there is minor uptake of nitrate and nitrite. Diffusion from groundwater can probably be ignored in the GOM as Rabalais et al. (2002) reported that the groundwater discharge is very low in coastal Louisiana, but is likely important elsewhere and is known to be important in the CSK. Based on this, we averaged and sum the fluxes data of nitrate, nitrite, and ammonium from McCarthy et al., 2015 for the GOM and Lee et al., 2012 for the CSK, respectively, and then applied $\boldsymbol{F_{Bott}^{DIN}}$ value as 1.2 mmol N m^{-2} day^{-1} in the GOM and 6.2 mmol N m^{-2} day^{-1} in the CSK. Thus, in equation 3, the benthic flux term is calculated from existing literature results after considering all DIN fluxes as above (Lee et al., 2012; McCarthy et al., 2015), and then multiplied by the area of each box.

The output terms are; 1) $\boldsymbol{F_{Export}^{DIN}}$, the exchange rate between each box in the lower layer, and 2) $\boldsymbol{F_{Deni}^{DIN}}$, the denitrification rate from the water column. Due to high stratification at the pycnocline, upward transfer of dissolved material from the lower layer to the upper layer is assumed not to occur in our model. Also, denitrification from the water column below the pycnocline is a significant N removal process, which removes up to a maximum 68% of total N input from the Mississippi River (MR) in the GOM (McCarthy et al., 2015). As the value of $\boldsymbol{F_{Deni}^{DIN}}$ in the GOM, we used a direct measurement of denitrification rates from the McCarthy et al., (2015) in the water column (88 μmol m^{-2} h^{-1}, which converted to 2.1 mmol N m^{-2} day^{-1}) where the stations were exactly same as our sub-region A, B, and C. We assumed this applied only below the pycnocline where oxygen concentrations decrease. However, in the CSK, there is no water column denitrification data because the dissolved oxygen concentration has never been down below about 4 mg L^{-1} during our data periods. Based on this, we estimated that

252 there is a very little water column denitrification in the CSK, so we did not count this term in the
253 CSK. Thus, we only considered the sedimentary denitrification term for the CSK region.
254 Water transport in the region is generally from the east, i.e., from near the Mississippi
255 River in Sub-region A to the west, near the Atchafalaya River in Sub-region C during non-
256 summer periods. During summer, the winds change direction from easterly to westerly,
257 blocking the water flow to the west (Cho et al., 1998). We calculated advection from current
258 meter data collected during the LATEX program (Nowlin et al., 1998a, b) from April 1992 to
259 December 1994, from which we determined U (west to east flow) and V (south to north flow)
260 components (cm s^{-1}). Figure 4 shows the mean values of coastal ocean current velocities. The
261 annual range of the currents is 0 to 30 cm s^{-1} for the longshore component, with standard
262 deviation of about 8 cm s^{-1}, and 0 to 7 cm s^{-1} for the cross-shelf component, with a similar
263 standard deviation, but these current velocities are not constant and change depending on time
264 and day. The annual current velocities in the CSK are more affected by tidal exchange and the
265 presence of the Yellow Sea Current, but velocities are similar to those in the GOM (Jacob et al.,
266 2000; Lim et al., 2008). The annual range of the currents is around 0 to 28 cm s^{-1} and 0 to 7 cm
267 s^{-1} for the cross-shelf component. Thus, we used the mean value of the current velocity for the
268 time of year during each cruise in both the GOM and the CSK for calculating the advective flow
269 in both alongshore and onshore/offshore directions.
270 To run the box model, we assumed three factors: 1) the study area is in a steady state
271 condition, with equal input sources and outputs, 2) AN-D is evenly distributed across each area,
272 and 3) DIN is fully utilized by phytoplankton growth in the layer above the pycnocline, so we
273 can neglect other removal factors. However, in the layer below the pycnocline, as we
274 mentioned above, denitrification, which leads to a main loss of DIN as nitrogen gas, is

considered as another output term in Equation 3. Because we assumed that all DIN removed is fully consumed by primary production above the pynocline, we can calculate potential carbon fluxes and oxygen consumption using the Redfield ratio (C: N: $-O_2$: P = 106: 16: 138: 1). The PPP can be compared with ^{14}C measurement data (Lohrenz et al., 1998, 1999; Redalje et al., 1994; Quigg et al., 2011) and dissolved oxygen data from MCH mooring C at 29° N, 92° W (4 March 2005 ~ 10 July 2005) (Bianchi et al., 2010).

Results

An N-mass balance model for the Texas-Louisiana Shelf

The existence of the three zones suggested by RC02 has been verified from winter data using nutrient/salinity relationships (Kim 2018). Figure 5 shows the contour graph based on the mean concentration of DIN at each station during the MCH M4 (March 2005) cruise. For operational and modeling purposes, stations were grouped into three sub-regions – near the Mississippi (A), near the Atchafalaya (C) and an intermediate region (B) between ~90°-91°W. During summer, it is hard to use nutrient/salinity relationships directly because riverine nutrient inputs are lower and phytoplankton growth causes rapid nutrient consumption over the shelf, leading to low overall nutrient surface concentrations. We calculated the mean [DIN] in each box, and then used the relationship between DIN and salinity to define the edges of the three zones. Near the coast salinity was consistently low, with high turbidity from the river water discharge. This was labelled the brown (river) zone.

A range of N input values from various sources were used in the N-mass balance model to estimate PPP and carbon fluxes in the coastal GOM. The PPP rates were highest near the river mouth and we set the boundaries of production for each zone based on our N-mass balance

298 model results and mean [DIN] data. We defined the brown zone as having the PPP rate of over
299 2 gC m^{-2} day^{-1} because of the high input of N from the river, AN-D, and benthic fluxes, and the
300 rate in the blue zone is less than 0.1 gC m^{-2} day^{-1}. The PPP rate in the green zone is then
301 between 0.1 and 2 gC m^{-2} day^{-1}. Basically, these PPP ranges were set based on synthesized
302 measured ranges of coastal GOM primary production, as defined for near, mid, and far fields of
303 the coastal GOM (Dagg and Breed 2003; Lohrenz et al., 1999). Note that our model results of
304 the PPP might overestimate the actual production because of light limitation, following RC02.
305 The edges of the three zones above and below the pycnocline layer, based on our N-mass
306 balance model results, are shown in Figures 6a and b. The patterns of the boundaries above and
307 below the pycnocline differ from the edges of the zones. The brown zone was found above the
308 pycnocline on all cruises close to the Mississippi River mouth because of the high nutrient
309 concentrations, but only appeared off the Atchafalaya River in March 2005 (MCH M4).
310 However, below the pycnocline it was found only in April 2004 (MCH M1) in sub-region A.
311 This suggests that vertical transport across the pycnocline rapidly removes the high levels of
312 suspended material that cause light limitation above the pycnocline. In the green zones, the
313 nutrient source is mostly supported directly by the river, with minor additional sources of N from
314 vertical sinking, AN-D, and benthic fluxes. We utilized the vertical sinking flux from the
315 sediment trap data from Qureshi (1995) below the pycnocline layer to estimate PPP. This
316 varied between 0.1-1.0 gN m^{-2} day^{-1} (Table 3). Typically, in the blue zone where biological
317 production is low, vertical sinking followed by local decomposition is assumed to be the major
318 factor that changes the nutrient concentration in the lower layer. The blue zone is always more
319 extensive below the pycnocline than above it, which suggests there is little or no sub-pycnocline
320 production except close to the coast and/or the river mouths, and reinforces the assumption that

any chlorophyll below the pycnocline is inactive (Figure 6b). Thus, we can identify the horizontal influence of the river plume in the layer below the pycnocline and the variation in the boundaries of the three zones, based on the observed nutrient data from a bottom layer and our N-mass balance model. The model suggests that regions of moderate potential productivity extend offshore at least as far as 28° 30'N in sub-region B, both above and below the pycnocline.

An N-mass balance model calibration

The model calibration was done with historic literature data. Literature data suggest that observed PP rates in the green and brown zones of the coastal GOM vary between 0.4 gC m^{-2} day^{-1} (winter) and ~ 8 gC m^{-2} day^{-1} (summer) (Dagg et al., 2007; Lohrenz et al., 1998, 1999; Redalje et al., 1994). Recently, Quigg et al. (2011) determined the integrated PP rates with ^{14}C measurements during 2004 in the coastal GOM. The highest integrated PP rates were found near the Mississippi River at 3.5 gC m^{-2} day^{-1} (in July), and near the Atchafalaya River at 2.7 ~ 5.9 gC m^{-2} day^{-1} (in May to July) (in the brown and green zones). However, lowest integrated PP rates were on the outer part of the LATEX shelf (the blue zone) at 0.07 gC m^{-2} day^{-1} (in March), 0.04 ~ 0.15 gC m^{-2} day^{-1} (in May), and 0.33 ~ 0.91 gC m^{-2} day^{-1} (in July). Additionally, Quigg et al., (2011) pointed out that these higher PP values were affected by high riverine nutrients input from the MR that flows westward during that time period.

The actual PP ranges were similar with our model-based PPP (Figure 6). However, this was different from RC02's brown zone. This might be due to the differences between methods such as ^{14}C, our N-mass balance model, and RC02's theoretical model. Typically, RC02 assumed that the brown zone is light limited due to high sediment turbidity, but our model does not account for this and only considered DIN concentrations. Except for this, our PPP results

344 are similar to direct productivity measurements from the ^{14}C incubations (Quigg et al., 2011).
345 Our model result (PPP) showed the same range of values as ^{14}C incubations (e.g., Dagg et al.,
346 2007; Lohrenz et al., 1998, 1999; Quigg et al., 2011; Redalje et al., 1994) in the three sub-
347 regions.

348 Note that our model assumed all the biological uptake could be converted directly to
349 production rates, which we considered as PPP. The PPP from cruises MCH M1 ~ M8 for
350 samples from above the pycnocline calculated using our model is reasonable based on
351 comparison with previous PP values (Figure 6a). The PPP ranges (0.01 ~ 5.05 gC m^{-2} day^{-1})
352 were similar to previous ^{14}C measurement PP values of between 0.04 ~ 5.9 gC m^{-2} day^{-1}.

353 Based on our model calculation, which assumes all the nutrients are available for
354 production, the PPP showed maxima at all times in sub-region A (near the Mississippi river) and
355 minima in sub-region B (between the Mississippi and Atchafalaya River), except for MCH M2
356 in June 2004, when sub-region C had the lowest PPP (Figure 6a). The high values in sub-
357 region A are due largely to underutilization of nutrients in regions of high turbidity. As the
358 water flows west under the influence of the Coriolis effect, PPP is expected to decrease as a
359 result of declining nutrient concentrations because of dilution and nutrient uptake during
360 biological production while the water flows to sub-region B. In sub-region C, MCH M4
361 (March 2005) had the highest PPP among the all MCH cruises. This probably depended on
362 high nutrient concentrations being present during the winter period, when the region was affected
363 by Atchafalaya River nutrient input.

364

365 *Model scenarios in the Gulf of Mexico (GOM)*

366 We tested the sensitivity of the model to changes in input/output parameters such as
367 increasing AN-D and decreasing riverine N input. Assuming the model is robust, we
368 investigated three model scenarios based on the nutrient distributions seen during the MCH1
369 cruise (note that using data from other cruises gives very similar results). In the first scenario,
370 we cut riverine N input 60% and increased the AN-D input by a factor of two based on
371 increasing N emission predictions (Duce et al., 2008; He et al., 2010; Kanakidou et al., 2016;
372 Kim (T) et al., 2011; Lawrence et al., 2000; Paerl et al., 2002). In the second scenario, we
373 doubled the amount of AN-D as in scenario 1 and decreased riverine N input by 30% based on
374 the hypoxia management plan goal (Gulf Hypoxia Action Plan Report, 2001, 2008; Rabalais et al.
375 2009). In the third scenario, we increased riverine N input by 20%, assuming the failure of the
376 hypoxia management plan, while we set the AN-D amount equal with the first and second
377 scenarios. Based on our N-mass balance model calculation and model scenarios, we can
378 initially estimate carbon fluxes from our PPP rate, and, using the Redfield carbon to oxygen
379 stoichiometry ratio (106:138), the overall oxygen balance within the coastal GOM (Table 4).
380 As can be seen in the scenario results for MCH M1 data (Table 4), the riverine N input
381 source is still the major controlling factor in the coastal GOM region even when its contribution
382 is greatly reduced and the AN-D source is doubled. For instance, if we fail to reduce riverine N
383 input in the future (scenario 3), the potential carbon fluxes will increase by 17% relative to
384 current conditions. In contrast, the AN-D input source only increased to a maximum of 5% of
385 the total input term and this indicates that AN-D input is still a minor factor in the GOM. If the
386 production is increased, overall oxygen demand will also be increased. The MCH M1 scenario
387 result indicated that the overall oxygen demand would increase approximately 21% if we fail to
388 reduce riverine N input, likely increasing considerably the area of the hypoxia.

389

390 *An N-mass balance model in the Coastal Sea off Korea (CSK)*

391 As we have done in the GOM, we used our N-mass balance model to estimate the PPP in
392 the CSK and define the three different zones (Figure 7). Similar to the GOM region, the PPP
393 rates were highest near the river mouth, and we set the boundaries of each zone based on our N-
394 mass balance model results. Based on nutrient data, as was done for the GOM, we defined the
395 brown zone as having a PPP rate above 1.5 gC m^{-2} day^{-1} because of the increased N sources from
396 the river, AN-D, and the sediment flux. We defined the green zone as having PPP rates
397 between 0.3 to 1.5 gC m^{-2} day^{-1} and the blue zone as having rates of less than 0.3 gC m^{-2} day^{-1}.

398 The seasonal results shown in Figures 7a and b show that the boundaries of the three
399 zones above and below the pycnocline layer were roughly consistent with the main change
400 coming in summer (August), which is the wet season and sees the highest river discharge. The
401 large size of the green zone in all seasons suggests that AN-D is consistently adding extra
402 nitrogen to the surface ocean along with the riverine N input. This is supported by the fact that
403 the PPP in the blue zone is an order of magnitude higher than for the GOM. Around 90% of the
404 grid cells in the CSK are in the same zones above and below the pycnocline (Figure 7 a and b)
405 during all four cruises; however, in the GOM (Figure 6 a and b) this was found for fewer than
406 half of the grid cells. This is probably due to the difference in freshwater discharge rate in the
407 two regions, which leads to a much larger stratified area in the GOM than in the CSK.

408 One question that has not been investigated is the temperature dependence of primary
409 productivity in the two areas. While the GOM is temperate throughout the year, winter
410 temperatures in the CSK fall to ~5°C. However, according to the ocean color remote sensing
411 images from near the CSK river mouth reported by Son et al., (2005), primary production in the

412 CSK does not appear to be strongly affected by temperature. The PPP results of our model (0.2
413 to 2.2 gC m^{-2} day^{-1}) agreed with their ocean color remote sensing results (0.4 to 1.6 gC m^{-2} day^{-1})
414 in the CSK. Also, during all seasons, the Keum River consistently supplies high amounts of
415 DIN (average: < 60 μM) (Lim et al., 2008) to the coastal zone (especially close to the Keum
416 mouth). We believe, therefore, that the higher value of PPP in winter near the Keum mouth
417 (brown zone in figure 7a), is reasonable.
418 The AN-D input source comes mainly from the Chinese side of the East China Sea (ECS)
419 and this affects the boundaries of the green and blue zones above the pycnocline as it is
420 deposited uniformly across the region. There is also nutrient input from offshore, as the Yellow
421 Sea Bottom Cold Water Mass can up-well during the mixing process and is assumed to supply
422 additional nutrients to the outer shelf (Lim et al., 2008).
423
424 *Model scenarios in Mid-Western Coastal Sea off Korea (CSK)*
425 AN-D is currently considerably more important (by approximately an order of magnitude)
426 in the CSK than in the GOM), and it is anticipated that AN-D will likely be a major controlling
427 factor here in the future (Duce et al., 2008; He et al., 2010; Kim (T) et al., 2011; Lawrence et al.,
428 2000; Paerl et al., 2002). Because of the lack of research on potential hypoxia scenarios in
429 Korea, we used the same three scenarios in the CSK as were used for the GOM. Similar to
430 GOM results, riverine N input remains the major controlling factor; however, in this area, the
431 AN-D source is more critical than in the GOM region (Table 5). The AN-D input source
432 increased from 20% to 47% of the total input under scenario 1, while based on our scenario 3
433 results, increases in the AN-D input source and riverine N input together will affect biological

434 production by increasing carbon fluxes up to 25% and oxygen demand up to 32% if we fail to
435 reduce N input in future (Table 5).
436
437 **Discussion**
438 Most previous model studies in the GOM were focused on predicting the hypoxia area
439 (Bierman et al., 1994; Fennel et al., 2011, 2013; Justic et al., 1996, 2002, 2003; Scavia et al.,
440 2004). For example, Justic et al., (1996; 2003) used a two-layer model incorporating vertical
441 oxygen data, from one station (LUMCON station C6; 28.867°N, 90.483°W), to predict the size
442 of the hypoxia area. Similarly, Fennel et al. (2011; 2013) used her more complex simulation
443 model, which included oxygen concentration as well as a plankton model from Fasham et al.
444 (1990), to predict the size of the hypoxia region in the GOM. Our N-mass balance model, in
445 contrast, uses historical data from the LATEX shelf to estimate potential carbon fluxes in the
446 GOM, and calculate the overall oxygen demand from those carbon fluxes. While this affects
447 the total area subject to hypoxia it does not estimate the size of the hypoxic zone.
448 In contrast to our model, traditional predictive models have also ignored different
449 nitrogen input sources such as AN-D and SGD. While this is probably reasonable on the
450 Texas-Louisiana shelf, where riverine inputs dominate, it may not apply in other coastal regions.
451 As a result, model studies in this region have concluded that reducing riverine N input is the only
452 solution to decrease the size of the hypoxia area in the GOM (Gulf Hypoxia Action Plan Report,
453 2001, 2008; Rabalais et al. 2009; Scavia et al., 2013). According to our model results, AN-D is
454 still a minor controlling factor in the GOM; however, in the CSK, the AN-D contributed more to
455 the total nitrogen budget and may be a major controlling factor in the future. This indicates that
456 AN-D should be considered as another input term for nutrient managements, especially in Asia

457 or in other regions where high concentrations are expected. Similarly, nitrogen input from
458 either sediment fluxes or groundwater also need to be considered.

459 Our zonal boundaries can be compared with the results of Lahiry (2007), who used
460 salinity to define the edges of each zone for the three cruises MCH M1, M2, and M3 (Figure 8)
461 and defined the edges of the RC02 zones in the coastal GOM based solely on salinity. Her
462 limited simulation results indicated similar patterns to our model based on DIN concentration
463 near the Mississippi River mouth (e.g., during MCH M1, M2, and M3). Mixing was more
464 conservative in this region than further west because the low salinity water with high nutrients
465 was less diluted with offshore water.

466 Away from the MR in sub-regions B and C, however, her results gave very different
467 boundaries for the three zones compared with our results (Figure 8). In particular, the results
468 near the Atchafalaya River were very different (compare Figures 6 and 8). For example, our
469 data showed only green and blue zones off Atchafalaya Bay during MCH M1, with no brown
470 zone. Similarly, the extent of the blue zones in sub-region C during MCH M2 and M3 is also
471 very different. We believe that our N-model based classification can cover more complex
472 biological processes than the Lahiry (2007) method, which considers only advection and mixing
473 and that our N-model is a more sensible way to look at biological processes in the GOM.

474 Our results also agree with previous studies that demonstrated that both the GOM and
475 CSK regions are N-limited for most of the year (Kim (G) et al., 2011; Turner and Rabalais,
476 2013). This compares with the results of Sylvan et al., (2007), who reported that the coastal
477 GOM could be P-limited in the MR delta mouth area where our brown zone is located, while
478 RC02 suggested light-limitation rather than N- or P-limitation. However, this P-limited
479 condition appears to occur when N concentrations are very high. In particular, the N/P ratios in

480 the both the GOM and CSK during our sampling were less than 16, indicating that both regions
481 were N-limited, although a few stations in the brown zone near the MR river area had ratios of
482 between 16 and 18 (Figure 9). These higher N to P ratios may result from the high sediment
483 turbidity causing light-limited conditions in this zone near the river mouth (Rowe and Chapman,
484 2002).

485 It should be remembered, however, that the arithmetic N:P value per se is unimportant in
486 determining nutrient limitation. As long as both nutrients can be measured, it is theoretically
487 possible for phytoplankton to continue to grow. The MARS has generally such an excess of N
488 relative to P that N:P ratios >>16 can be expected as P concentrations fall, but this does not
489 necessarily mean that productivity is limited, and we never found P concentrations of zero in any
490 of our sub-regions; the lowest P concentration measured during all cruises in the GOM and CSK
491 was 0.2 μM.

492 Both the GOM and CSK regions receive nitrogen inputs from AN-D, rivers, and benthic
493 fluxes. These different nitrogen input sources control coastal productivity, and this may reflect
494 the different nitrogen cycling in the two regions. In the GOM, the riverine N input source
495 consistently dominates coastal productivity and eutrophication, while, in the CSK, AN-D is also
496 becoming a critical controlling factor. In the CSK, however, there is strong tidal mixing of
497 freshwater from the Keum River and/or Gyunggi Bay with nearby coastal water, which results in
498 a tidal front along the offshore region and off the Taean Peninsula during spring and summer.
499 It is this physical mixing that mostly controls the spatial distribution patterns of nutrients and
500 salinity here, particularly below the pycnocline (Lim et al., 2008). The brown zone in the upper
501 layer in the CSK (August 2008) changed to a green zone region below the pycnocline layer as a
502 result of the strong coastal tidal mixing.

503 RC02 considered their model to be theoretical. In the brown zone, close to the river
504 mouth, they assumed turbidity leads to light-limited conditions. Their results agree well with
505 measured ^{14}C PP numbers from Quigg et al. (2011) who found the lowest integrated PP is near
506 the MR delta mouth. However, our N-mass balance model did not consider light limitation and
507 therefore PPP in the brown zone is high. Such good agreement suggests that our model can be
508 applied to a wide region, while ^{14}C measurements are typically conducted at a few specific points,
509 as long as such limitations are taken into account.

510 In the CSK, most previous production studies focused on inshore areas such as estuaries
511 or rivers. Our research focused for the first time on the coastal ocean off Korea. Our results
512 suggest that diverse nitrogen sources need to be recognized as potential issues for future nutrient
513 management concerned with hypoxia, eutrophication, or other environmental issues. The
514 agreement between our results and the pattern of production based on satellite-sensing in the
515 CSK (Son et al., 2005), suggests that our model is reasonable.

516 The results of our changing scenarios represent how the biological processes in these
517 coastal regions may vary as individual nutrient sources change. While our model cannot
518 predict the area of the hypoxic zone, we can investigate the effects of potential flux changes of
519 each factor, such as AN-D, riverine input, or benthic fluxes, and calculate the effects of changes
520 in each on PPP and on the overall oxygen balance for the region. We have only considered
521 different input terms of our N-mass balance model; output terms such as water mixing rates and
522 the residence time for each box need more detailed study in future work to calculate more
523 realistic production changes in each box.

524

525 **Conclusion**

526 The model suggests that the three zone theory of RC02 can be applied not only in the
527 northern GOM but also in the CSK region and that three zones can be distinguished based on
528 their nutrient concentration. As a result, we believe that using our N-mass balance model to
529 separate different zones based on RC02 may be appropriate not only for large-scale regions like
530 the GOM and CSK but also at small scales such as river or estuary systems. The model also
531 estimates potential primary production and carbon flux based on the inclusion of AN-D data that
532 have not been considered previously (e.g. Bierman et al., 1994; Kim (T) et al., 2011). Our
533 results agree well with previous ^{14}C measurements in the GOM (Quigg et al., 2011) and ocean
534 color remote sensing in the CSK (Son et al., 2005).
535 Based on CSK cruise data results, we can initially determine where the three different
536 zones are in the CSK. We evaluated our model and tested its sensitivity based on three
537 different scenarios. Through our scenario results, we assume that the AN-D is a considerable
538 factor in the CSK as well as the riverine N input from the Keum river. Reducing nutrient input
539 from the river is critical for hypoxia management policy (Gulf Hypoxia Action Plan Report,
540 2001, 2008; Rabalais et al. 2009). In addition, these model scenarios will be helpful in future
541 coastal nutrient management or hypoxia management studies in the CSK, especially as AN-D
542 sources become more important.
543
544 **Acknowledgements**
545 The authors would like to thank to the captain and crew of the R/V Gyre, R/V Pelican,
546 and R/V Manta along with the many marine technicians and students who participated in the
547 cruises. This research was made possible by grant SA 12-09/GoMRI-006 to the Gulf Integrated
548 Spill Consortium from the Gulf of Mexico Research Initiative and by grants NA03NOS4780039,

549 NA06NOS4780198, and NA09NOS4780208 from NOAA. Hydrographic and dissolved
550 nutrients data used in this study from the Texas-Louisiana Shelf from years 2004-2009 are
551 available from NOAA NCEI (accession-ID 0088164).
552

References

Anderson, G. C.: Subsurface chlorophyll maximum in the northeast Pacific Ocean. Limnology and Oceanography., 14(3), 386-391, 1969.

Alexander, R. B., Smith, R. A., Schwartz, G. E., Preston, S. D., Brakebill, J. W., Srinivasan, R., and Pacheco, A. P.: Atmospheric nitrogen flux from the watersheds of major estuaries of the United States: An application of the SPARROW watershed model, in: Coastal and Estuarine Studies-Nitrogen Loading in Coastal Water Bodies: An Atmospheric Perspective, edited by: Valigura, R. A., Alexander, R. B., Castro, M. S., Meyers, T. P., Paerl, H. W., Stacey, P. E., Turner, R. E., American Geophysical Union, Washington, D.C., USA, 119-170, 2001.

Alexander, R. B., Smith, R. A., Schwarz, G. E., Boyer, E. W., Nolan, J. V., and Brakebill, J. W.: Differences in phosphorus and nitrogen delivery to the Gulf of Mexico from the Mississippi river basin. Environmental Science and Technology., 42, 822-830, 2008.

Belabbassi, L.: Examination of the relationship of river water to occurrences of bottom water with reduced oxygen concentrations in the northern Gulf of Mexico. Texas A & M University. Ph.D. Dissertation., 2006.

Bianchi, T. S., DiMarco, S. F., Cowan, Jr. JH., Hetland, R. D., Chapman, P., Day, J. W., and Allison, M. A.: The Science of hypoxia in the Northern Gulf of Mexico: A review. Science of the total Environment., 408(7), 1471-1484, 2010.

Bierman, V. J., Hinz, S. C., Wiseman, Jr. W. J., Rabalais, N. N., and Turner, R. E.: A Preliminary Mass Balance Model of Primary Productivity and Dissolved Oxygen in the Mississippi River Plume/Inner Gulf Shelf Region. Estuaries., 17(4), 886-899, 1994.

Bode, A., and Dortch, Q.: Uptake and regeneration of inorganic nitrogen in coastal waters influenced by the Mississippi River: spatial and seasonal variations. Journal of Plankton Resources., 18, 2251-2268, 1996.

Castro, M. S., Driscoll, C. T., Jordan, T. W., Reay, W. G., Boynton, W. R., Seitzinger, S. P., Styles, R. V., and Cable, J. E.: Contribution of atmospheric deposition to the total nitrogen loads to thirty-four estuaries on the Atlantic and Gulf coasts of the United States, in: Coastal and Estuarine Studies-Nitrogen Loading in Coastal Water Bodies: An Atmospheric Perspective, edited by: Valigura, R. A., Alexander, R. B., Castro, M. S., Meyers, T. P., Paerl, H. W., Stacey, P. E., Turner, R. E., American Geophysical Union, Washington, D.C., USA, 77-106, 2001.

Castro, M. S., and Driscoll, C. T.: Atmospheric nitrogen deposition to estuaries in the mid-Atlantic and northeastern United States. Environmental science & technology., 36(15), 3242-9, 2002.

Cho, K. R., Reid, O., and Nowlin, Jr W. D.: Objectively mapped stream function fields on the Texas-Louisana shelf based on 32 months of moored current meter data. Journal of Geophysics Research., 103(C5), 10377-10390, 1998.

Choi, H. Y., Lee, S. H., and Oh, I. S.: Quantitative Analysis of the Thermal Front in the Mid-Eastern Coastal Area of the Yellow Sea. Journal of the Korean Society of Oceanography [The Sea]., 3, 1-8, 1998.

Choi, H. Y., Lee, S. H., and Yoo, K. Y.: Salinity Distribution in the Mid-eastern Yellow Sea during the High Discharge from the Keum River Weir. Journal of the Korean Society of Oceanography [The Sea]., 4, 1-9, 1999.

Christensen, P. B., Rysgaard, S., Sloth, N. P., Dalsgaard, T., and Schwaerter, S.: Sediment mineralization, nutrient fluxes, denitrification and dissimilatory nitrate reduction to ammonium in an estuarine fjord with sea cage trout farms. Aquatic Microbial Ecology., 21, 73-84, 2000.

Cornell, S., Rendell, A., and Jickells, T.: Atmospheric inputs of dissolved organic nitrogen to the oceans. Nature., 376, 243-246, 1995.

Dagg, M. J., and Breed, G. A.: Biological effects of Mississippi River nitrogen on the northern Gulf of Mexico-a review and synthesis. Journal of Marine Systems., 43, 133-152, 2003.

Dagg, M. J., Ammerman, J. W., AMON, R. M. W., Gardner, W. S., Green, R. E., Lohrenz, S. E.: A review of water column processes influencing hypoxia in the northern Gulf of Mexico. Estuaries Coasts., 30, 735-752, 2007.

Dalsgaard, T.: Benthic primary production and nutrient cycling in sediments with benthic microalgae and transient accumulation of macroalgae. Limnology and Oceanography., 48(6), 2138-2150, 2003.

De Boer, A. M., Watson, A. J., Edwards, N. R., and Oliver, K. I. C.: A multi-variable box model approach to the soft tissue carbon pump. Climate of the past., 6, 827-841, 2010.

Diaz, R. J., and Rosenberg, R.: Marine benthic hypoxia: A review of its ecological effects and the behavioural responses of benthic macrofauna. Oceanography Marine Biology. Ann. Rev., 33, 245-303, 1995.

Diaz, R. J., and Rosenberg, R.: Spreading dead zones and consequences for marine ecosystems. Science., 321(5891), 926-9, 2008.

DiMarco, S. F., and Zimmerle, H. M.: MCH Atlas: Oceanographic Observations of the Mechanisms Controlling Hypoxia Project. Texas A&M University, Texas Sea Grant, College Station, TX. Publication TAMU-SG- 17-601,350. ISBN 978-0-692-87961-0, 2017.

643 DiMarco, S. F., Chapman, P., Walker, N., and Hetland, R. D.: Does local topography control
644 hypoxia of the Texas-Louisiana Shelf? Journal of Marine Systems., 80(1-2), 25-35, 2010.
645
646 Dodds, W. K., and Smith, V. H.: Nitrogen, phosphorus, and eutrophication in streams. Inland
647 Waters., 6, 155-164, 2016.
648
649 Doney, S. C., Mahowald, N., Lima, L., Feely, R. A., Mackenzie, F. T., Lamarque, J. F., and
650 Rasch, P. J.: Impact of anthropogenic atmospheric nitrogen and sulfur deposition on
651 ocean acidification and the inorganic carbon system. Proceedings of the National
652 Academy of Science., 104, 14580-14585, 2007.
653
654 Dortch, Q., and Whitledge, T. E.: Does nitrogen or silicon limit phytoplankton in the Mississippi
655 River plume and nearby regions? Continental Shelf Research., 12, 1293-1309, 1992.
656
657 Duce, R. A., LaRoche, J., Altierl, K., Arrigo, K. R., Baker, A. R., Capone, D. G., Cornell, S.,
658 Dentener, F., Galloway, J., Ganeshram, R. S., Geider, R. J., Jickells, T., Kuypers, M. M.,
659 Langlois, R., Liss, P. S., Liu, S. M., Middelburg, J. J., Moore, C. M., Nickovic, S.,
660 Oschlies, A., Pedersen, T., Prospero, J., Schlitzer, R., Seitzinger, S., Sorensen, L. L.,
661 Uematsu, M., Ulloa, O., Voss, M., Ward, B., and Zamora, L.: Impacts of Atmospheric
662 Anthropogenic Nitrogen on the Open Ocean. Science., 320, 893-897, 2008.
663
664 Fasham, M. J. R., Ducklow, H. W., and Mckelvie, S. M.: A nitrogen-based model of plankton
665 dynamics in the oceanic mixed layer. Journal of Marine research., 48, 591-639, 1990.
666
667 Feng, Y., DiMarco, S. F., and Jackson, G. A.: Relative role of wind forcing and riverine nutrient
668 input on the extent of hypoxia in the northern Gulf of Mexico. Geophysical Research
669 Letters., 39, L09601, 2012.
670
671 Feng, Y., Fennel, K., Jackson, G. A., DiMarco, S. F., and Hetland, R. D.: A model study of the
672 response of hypoxia to upwelling-favorable wind on the northern Gulf of Mexico shelf.
673 Journal of Marine Systems., 131, 63-73, 2014.
674
675 Fennel, K., Wilkin, J., Levin, J., Moisan, J., O'Reilly, J., and Haidvogel, D.: Nitrogen cycling in
676 the Middle Atlantic Bight: Results from a three-dimensional model and implications for
677 the North Atlantic nitrogen budget. Global Biogeochemical cycles., 20, GB3007,
678 doi:10.1029/2005G, 2006.
679
680 Fennel, K., Hetland, R. D., Feng, Y., and DiMarco, S. F.: A coupled physical-biological model
681 of the Northern Gulf of Mexico shelf: model description, validation and analysis of
682 phytoplankton variability. Biogeosciences., 8, 1881-1899, 2011.
683
684 Fennel, K., Hu, J., Laurent, A., Marta-Almeida, M., and Hetland, D. R.: Sensitivity of hypoxia
685 predictions for the northern Gulf of Mexico to sediment oxygen consumption and model
686 nesting. Journal of Geophysical Research: Oceans., 118, 990-1002, 2013.
687

Forrest, D. R., Hetlandl R. D., and DiMarco, S. F.: Multivariable statistical regression models of the areal extent of hypoxia over the Texas–Louisiana continental shelf. Environmental Research Letters., 6, 045002, 2011.

Goolsby, D. A. Mississippi basin nitrogen flux believed to cause Gulf hypoxia., EOS Transactions 2000:29–321, 2000.

Green, R. E., Gould, Jr. R. W., and Ko, D. S.: Statistical models for sediment/detritus and dissolved absorption coefficients in coastal waters of the northern Gulf of Mexico. Continental Shelf Research., 28(10), 1273-1285, 2008.

Hagy, J. D., Sanford, L. P., and Boynton. W. R.: Estimation of net physical transport and hydraulic residence times for a coastal plain estuary using box models., Estuaries 23:328–340. doi:10.2307/1353325, 2000.

He, C. H., Wang, X., Liu, X., Fangmeler, A., Christie, P., and Zhang, F.: Nitrogen deposition and its contribution to nutrient inputs to intensively managed agricultural ecosystems. Ecological Application., 20(1), 80-90, 2010.

Hetland, R. D., and DiMarco, S. F.: How does the character of oxygen demand control the structure of hypoxia on the Texas-Louisiana continental shelf? Journal of Marine Systems., 70, 49-62, 2008.

Howarth, R. W., and Marino, R.: Nitrogen as the limiting nutrient for eutrophication in coastal marine ecosystems: Evolving views over three decades. Limnology and Oceanography., 51(1), 364-376, 2006.

Jacob, G. A., Hur, H. B., and Riedlinger, S. K.: Yellow and East China Seas response to winds and currents. Journals of Geophysical Research., 105 (21), 947-968, 2000.

Justic, D., Rabalais, N. N., and Turner, R. E.: Effects of climate change on hypoxia in coastal waters; A doubled CO2 scenario for the northern Gulf of Mexico. Limnology and Oceanography., 41(5), 992-1003, 1996.

Justic, D., Rabalais, N. N., and Turner, R. E.: Modeling the impacts of decadal changes in riverine nutrient fluxes on coastal eutrophication near the Mississippi River Delta. Ecological Modelling., 152, 33-46, 2002.

Justic, D., Rabalais, N. N., and Turner, R. E.: Simulated responses of the Gulf of Mexico hypoxia to variations in climate and anthropogenic nutrient loading. Journal of Marine Systems., 42, 115-126, 2003.

Kanakidou, M., Myriokefalitakis, S., Daskalakis, N., and Fanourgakis, G.: Past, Present, and Future Atmospheric Nitrogen Deposition. American Meteorological Society. Journal of the Atmospheric Sciences., 73(5), 2039-2047, 2016.

734 Kim, G., Kim, J. S., and Hwang, D. W.: Submarine groundwater discharge from oceanic islands
735 standing in oligotrophic oceans: Implications for global production and organic carbon
736 fluxes. Limnology and Oceanography., 56(2), 673-682, 2011.
737
738 Kim, J. S., Lee, M. J., Kim, J., and Kim, G.: Measurement of Temporal and Horizontal
739 Variations in ^{222}Rn Activity in Estuarine Waters for Tracing Groundwater Inputs.
740 Ocean Science Journal., 45(4), 197-202, 2010.
741
742 Kim, J. S.: Implications of different nitrogen input sources for primary production and carbon
743 flux estimates in coastal waters. Texas A&M University. Ph.D. Dissertation., 2018.
744
745 Kim, J. Y., Ghim, Y. S., Lee, S. B., Moon, K. C., Shim, S. G., Bae, G. N., and Yoon, S. C.:
746 Atmospheric Deposition of Nitrogen and Sulfur in the Yellow Sea Region: Significance
747 of Long-Range Transport in East Asia. Water, Air, and Soil Pollution., 205, 259-272,
748 2010.
749
750 Kim, T. W., Lee, K., Najjar, R. G., Jeong, H. D., and Jeong, H. J.: Increasing N abundance in the
751 northwestern Pacific Ocean due to atmospheric nitrogen deposition. Science., 334, 505-
752 509, 2011.
753
754 Lahiry, S.: Relationships between nutrients and dissolved oxygen concentrations on the Texas-
755 Louisiana shelf during spring-summer of 2004. Texas A & M University. MS. Thesis.,
756 2007.
757
758 Lamarque, J. F., Dentener, F., McConnell. J., Ro. C. U., Shaw. M., Vet. R., Bergmann. D.,
759 Cameron-Smith. P., Dalsoren. S., Doherty. R., Faluvegi. G., Ghan. S. J., Josse. B., Lee. Y.
760 H., MacKenzie. I. A., Plummer. D., Shindell. D. T., Skeie. R. B., Stevenson. D. S., Strode.
761 S., Zeng. G., Curran. M., Dahl-Jensen. D., Das. S., Fritzsche. D., and Nolan. M.: Multi-
762 model mean nitrogen and sulfur deposition from the Atmospheric Chemistry and Climate
763 Model Intercomparison Project (ACCMIP): evaluation of historical and projected future
764 changes. Atmospheric Chemistry and Physics., 13, 7997-8018, 2013.
765
766 Lawrence, G. B., Goolsby, D. A., Battaglin, W. A., and Stensland, G. J.: Atmospheric nitrogen in
767 the Mississippi River Basin-emissions, deposition and transport. Science of The Total
768 Environment., 248(2-3), 87-100, 2000.
769
770 Laurent, A., Fennel, K., Hu, J., and Hetland, R. D.: Simulating the effects of phosphorus
771 limitation in the Mississippi and Atchafalaya River plumes. Biogeosciences., 9, 4797-
772 4723, 2012.
773
774 Lee, J. S., Kim, K. H., Shim, J. H., Han, J. H., Choi, Y. H., and Khang, B. J.: Massive
775 sedimentation of fine sediment with organic matter and enhanced benthic-pelagic
776 coupling by an artificial dyke in semi-enclosed Chonsu Bay, Korea. Marine Pollution
777 Bulletin., 64, 153-163, 2012.
778

779 Lim, D., Kang, M. R., Jang, P. G., Kim, S. Y., Jung, H. S., Kang, Y. S., and Kang, U. S.: Water
780 Quality Characteristics Along Mid-Western Coastal Area of Korea. Ocean and Polar
781 Research., 30(4), 379-399, 2008.
782
783 Liu, S. M., Zhang, J., Chen, S. Z., Chen, H. T., Hong, G. H., Wei, H., and Wu, Q. M.: Inventory
784 of nutrient compounds in the Yellow Sea. Continental Shelf Research., 23, 1161-1174,
785 2003.
786
787 Lehrter, J. C., Beddick Jr., D. L., Devereux, R., Yates, D. F., and Murrell. M. C.: Sediment-water
788 fluxes of dissolved inorganic carbon, O_2, nutrients, and N_2 from the hypoxic region of
789 the Louisiana continental shelf. Biogeochemistry, 109, 233–252, 2012.
790
791 Lohrenz, S. E., Wiesenburg, D. A., Arnone, R. A., and Chen, X. G.: What controls primary
792 production in the Gulf of Mexico? In: Sherman K, Kumpf H, Steidinger K (ed) The Gulf
793 of Mexico Large Marine Ecosystem: Assessment, sustainability and management.
794 Blackwell Science, Malden, MA., 151-170, 1998.
795
796 Lohrenz, S. E., Fahnenstiel, G. L., Redalje, D. G., Lang, G. A., Dagg, M. J., Whitledge, T. E.,
797 and Dortch, Q.: Nutrients, irradiance, and mixing as factors regulating primary
798 production in coastal waters impacted by the Mississippi River plume. Continental Shelf
799 Research., 19, 1113-1141, 1999.
800
801 Luo, X. S., Tang, A. H., Shi, K., Wu, L. H., Li, W. Q., Shi, W. Q., Shi, X. K., Erisman, J. W.,
802 Zhang, F. S., and Liu, X. J.: Chinese coastal seas are facing heavy atmospheric nitrogen
803 deposition. Environmental Research Letters., 9, 1-10, 2014.
804
805 McCarthy, M. J., Newell, S. E., Carini, S. A., and Cardner, W. S.: Denitrification dominates
806 sediment nitrogen removal and is enhanced by bottom-water hypoxia in the Northern
807 Gulf of Mexico. Estuaries and Coasts., 38, 2279-2294. 2015.
808
809 Milliman, J. D., and Meade, R. H.: World-wide delivery of river sediment to the oceans. The
810 Journal of Geology., 91(1), 1-21, 1983.
811
812 Mississippi River/Gulf of Mexico Watershed Nutrient Task Force.: Action Plan for Reducing,
813 Mitigating, and Controlling Hypoxia in the Northern Gulf of Mexico, Washington, D.C.
814 33 pp., 2001.
815
816 Mississippi River/Gulf of Mexico Watershed Nutrient Task Force.: Gulf Hypoxia Action Plan
817 2008 for Reducing, Mitigating, and Controlling Hypoxia in the Northern Gulf of Mexico
818 and Improving Water Quality in the Mississippi River Basin, Washington, D.C. 61 pp.,
819 2008.
820
821 Nipper, M., Sanchez Chavez, J. A., Tunnell, Jr. J. W.: GulfBase: Resource Database for Gulf of
822 Mexico Research: Corpus Christi, Texas A&M University, http://www.gulfbase.org,
823 2004.
824

Nowlin, W. D. Jr., Jochens, A. E., Reid, R. O., and DiMarco, S. F.: Texas-Louisiana Shelf Circulation and Transport processes Study: Synthesis Report, Volume I: Technical Report. OCS Study MMS 98-0035. U.S. Dept. of the Interior, Minerals Mgmt Service, Gulf of Mexico OCS Region, New Orleans, LA., 502, 1998a.

Nowlin, W. D. Jr., Jochens, A. E., Reid, R. O., and DiMarco, S. F.: Texas-Louisiana Shelf Circulation and Transport processes Study: Synthesis Report, Volume II: Appendices. OCS Study MMS 98-0036. U.S. Dept. of the Interior, Minerals Mgmt Service, Gulf of Mexico OCS Region, New Orleans, LA., 288, 1998b.

Nunnally, C., Quigg, A., DiMarco, S. F., Chapman, P., and Rowe, G. T.: Benthic-Pelagic Coupling in the Gulf of Mexico Hypoxic Area: Sedimentary enhancement of hypoxic conditions and near bottom primary production. Continental Shelf Research., 85, 143-152, 2014.

Paerl, H. W., Dennis, R. L., and Whitall, D. R.: Atmospheric Deposition of Nitrogen: Implications for Nutrient Over-Enrichment of Coastal Waters. Estuaries., 25(4B), 677-693, 2002.

Paerl, H. W.: Controlling Eutrophication along the Freshwater-Marine Continuum: Dual Nutrient (N and P) Reductions are Essential. Estuaries and Coasts., 32, 593-601, 2009.

Park, M. J., Savenije, H. H. G., Cai, H., Jee, E. K., and Kim, N. H.: Progressive change of tidal wave characteristics from the eastern Yellow Sea to the Asan Bay, a strongly convergent bay in the west coast of Korea. Ocean Dynamics., 67, 1137-1150, 2017.

Park, Y. H.: Analysis of characteristics of Dynamic Tidal Power on the west coast of Korea. Renewable and Sustainable Energy Reviews., 68, 461-474, 2017.

Qureshi, N. A.: The role of fecal pellets in the flux of carbon to the sea floor on a river-influenced continental shelf subject to hypoxia. Louisiana State University. Ph.D. Dissertation., 1995.

Quigg, A., Sylvan, J., Gustafson, A., Fisher, T., Oliver, R., Tozzi, S., and Ammerman, J.: Going west: nutrient limitation of primary production in the northern Gulf of Mexico and the importance of the Atchafalaya River. Aquatic Geochemistry., 17, 519-544, 2011.

Rabalais, N. N., and Smith, L. E.: The effects of bottom water hypoxia on benthic communities of the southeastern Louisiana continental shelf. New Orleans, Louisiana, U.S. Minerals Management Service, Gulf of Mexico OCS Region.,105, 1995.

Rabalais, N. N., and Turner, R. E.: Hypoxia in the Northern Gulf of Mexico: Description, causes and change, pp. 1–36. In N. N. Rabalais and R. E. Turner (eds.), Coastal Hypoxia: Consequences for Living Resources and Ecosystems. Coastal and Estuarine Studies., 58, 2001.

Rabalais, N. N., Turner, R. E., and Scavia, D.: Beyond science into policy: Gulf of Mexico hypoxia and the Mississippi river. Bioscience., 52(2), 129-142, 2002.

Rabalais, N. N., Turner, R. E., Sen Gupta, B. K., Boesch, D. F., Chapman, P., and Murrell, M. C.: Hypoxia in the northern Gulf of Mexico: Does the science support the plan to reduce, mitigate, and control hypoxia? Estuaries Coastal., 30, 753-772, 2007.

Rabalais, N. N., Turner, R. E., Justic, D., Diaz, R. J.: Global change and eutrophication of coastal waters. ICES. Journal of Marine Science., 66, 1528–1537, 2009.

Ramesh. R., Chen. Z., Cummins. V., Day. J., D'Elia. C., Dennison. B., Forbes. D. L., Glaeser. B., Claser. M., Clavovic. B., Kremer. H., Lange. M., Larsen. J. N., Tissier. M. Le., Newton. A., Pelling. M., Purvaja. R., and Wolanski. E.: Land-ocean interactions in the coastal zone: past, present & future, Anthtropocene., 12, 85-98, 2015.

Redalje, D. G., Lohrenz, S. E., and Fahnenstiel, G. L.: The relationship between primary production and the vertical export of particulate organic matter in a river impacted coastal ecosystem. Estuaries., 17, 829-838, 1994.

Robertson, D. M., and Saad, D. A.: SPARROW Models Used to Understand Nutrient Sources in the Mississippi/Atchafalaya River Basin. Journal of Environmental Quality., 42, 1422-1440, 2014.

Rowe, G. T., and Chapman, P.: Continental Shelf Hypoxia: some nagging questions. Gulf Mexico Science., 20, 153-160, 2002.

Rowe, G. T., Kaegi, M. E. C., Morse, J. W., Boland, G. S., and Briones, E. G. E.: Sediment community metabolism associated with continental shelf hypoxia, northern Gulf of Mexico. Estuaries., 25(6), 1097–1106, 2002.

Scavia, D., Justic, D., and Bierman, V. J.: Reducing Hypoxia in the Gulf of Mexico: Advice from Three Models. Estuaries., 27(3), 419-425. 2004.

Scavia, D., Evans, M. A., and Obenour, D. R.: A scenario and forecast model for Gulf of Mexico hypoxic area and volume. Environmental Science and Technology., 47, 10423-10428, 2013.

Shou, W., Zong, H., Ding, P., and Hou, L.: A modelling approach to assess the effects of atmospheric nitrogen deposition on the marine ecosystem in the Bohai Sea, China. Estuarine, Coastal and Shelf Science., 208, 36-48, 2018.

Sigman, D. M., and Hain, M. P.: The Biological Productivity of the Ocean. Nature Education., 3, 1-16, 2012.

915 Son, S. H., Campbell, J. W., Dowell, M., Yoo, S. J., and Noh, J.: Primary production in the
916 Yellow Sea determined by ocean color remote sensing. Marine Ecology Progress Series.,
917 303, 91-103, 2005.
918
919 Sylvan, J. B., Dortch, Q., Nelson, D. M., Maier Brown, A. F., Morrison, W., Ammerman, J. W.:
920 Phosphorus limits phytoplankton growth on the Louisiana shelf during the period of
921 hypoxia formation. Environmental Science and Technology., 40(24), 7548– 7553, 2006.
922
923 Testa, J. M., Kemp. W. M., Boynton. W. R., and Hagy. J. D: Long-term changes in water quality
924 and productivity in the Patuxent river estuary: 1985 to 2003. Estuaries and Coasts., 31,
925 1021-1037, 2008.
926
927 Thornton, D. C. O., Dong, L. F., Underwood, G. J. C., and Nedwell, D. B.: Sediment-water
928 inorganic nutrient exchange and nitrogen budgets in the Colne Estuary, UK. Marine
929 Ecology Progress Series., 337, 63-77, 2007.
930
931 Turner, R. E., and Rabalais, N. N.: Changes in the Mississippi River nutrient supply and offshore
932 silicate-based phytoplankton community responses, in: Changes in Fluxes in Estuaries:
933 Implications from Science to management Proceedings of ECSA22/ERF Symposium.
934 International Symposium Series, Olsen, Gredensborg, Denmark.,147-150, 1994.
935
936 Turner, R. E., Rabalais, N. N., and Justic, D.: Predicting summer hypoxia in the northern Gulf of
937 Mexico: riverine N, P and Si loading. Marine Pollution Bulletin., 51, 139-148, 2006.
938
939 Turner, R. E., Rabalais, N. N., and Justic, D.: Gulf of Mexico Hypoxia: Alternate States and a
940 Legacy. Environmental Science & Technology., 42, 2323-2327, 2008.
941
942 Turner, R. E., and Rabalais, N. N.: Nitrogen and phosphorus phytoplankton growth limitation in
943 the northern Gulf of Mexico. Aquatic microbial ecology., 68, 159–169, 2013.
944
945 Wade, T. L., and Sweet, S. T.: Final Report Coastal Bend Bays and Estuaries Program (CBBEP):
946 Atmospheric Deposition Study, Coastal Bend Bays & Estuaries Program, Corpus Christi,
947 Texas, USA, 48 pp, 2008.
948
949 Wang, H., Dai, M., Liu, J., Kao, S. J., Zhang, C., Cai, W. J., Wang, G., Qian, W., Zhao, M., and
950 Sun, Z.: Eutrophication-Driven Hypoxia in the East China Sea off the Changjiang
951 Estuary. Environmental Science & Technology., 50, 2255-2263, 2016.
952
953 Yang, J. S., and Ahn, T. Y.: The analysis of the correlation between groundwater level and the
954 moving average of precipitation in Kuem river watershed. The Journal of Engineering
955 Geology., 18, 1-6, 2008.
956
957 Zhao, Y., Zhang, L., Pan, Y., Wang, Y., Paulot, F., and Henze, D. K.: Atmospheric nitrogen
958 deposition to the northwestern Pacific: seasonal variation and source attribution. Atmos.
959 Chem. Phys., 15, 10905-10924, 2015.
960

961 **List of Figures**

962 Figure 1. Study sites and sampling areas in the Gulf of Mexico and Korea. (a) shows the
963 sampling area within the northern Gulf of Mexico. Flow in the Mississippi/
964 Atchafalaya River System is split 30% to the Atchafalaya River, 70% to the Mississippi
965 River. The box is the sampling area. (b) shows station positions from March 2005.
966 Note that MCH project data are widely distributed across the region. Red, grey, and
967 blue stations correspond to sub-regions A (near the Mississippi River), B (between the
968 Mississippi and Atchafalaya), and C (near the Atchafalaya) respectively. (c) shows
969 the sampling area off the west coast of Korea. (d) shows all of the station positions.
970
971 Figure 2. The Rowe and Chapman three zone hypothesis, which describes the physical and
972 biochemical processes that initiate and sustain hypoxia on the Texas-Louisiana Shelf,
973 [Rowe and Chapman, 2002]. RMEPs are Reduced Metabolic End Products.
974 *Reprinted with permission of Gulf of Mexico Science.*
975
976 Figure 3. (a) Input (blue) and output (red) sources for each 0.25° box in the GOM and CSK (see
977 text for details); (b) Area of each sub-region (red) and boxes affected by direct riverine
978 input (blue) in the GOM. Export N (Mixing) represents the advective transport term.
979 The processes of biogeochemical and transport processes of both regions are the same
980 and each in/out put factor is the same in the GOM and CSK. Note that transfer
981 between boxes occurs in both directions alongshore and onshore/offshore and is not a
982 one-dimensional process as suggested in the diagram.
983
984 Figure 4. Mean ocean current velocities (a) and standard deviations (b) for biweekly periods
985 from August 1993 through December 1994 based on data from LATEX project.
986 Positive values of U show eastward flow; positive values of V show northward flow.
987
988 Figure 5. Extent of the three zones defined by RC02 based on the mean concentration of nutrient
989 (DIN) at each station during the MCH M4 cruise in March 2005, showing their
990 correspondence to the three sub-regions used in the box model. Red, grey and blue
991 stations correspond to sub-regions A (near the Mississippi River), B (between the
992 Mississippi and Atchafalaya), and C (near the Atchafalaya) respectively.
993
994 Figure 6a. Areal distributions of the three zones using data from above the pycnocline, based on
995 N-mass balance model results. Colors and numbers represent boxes found in each of
996 the three zones in terms of potential productivity (Unit: gC m^{-2} day^{-1}).
997
998 Figure 6b. As for 6a, using data from below the pycnocline.
999
1000 Figure 7a. The distribution of the three zones off Mid-western Korea (CSK) above the
1001 pycnocline based on the RC02 hypothesis applied to the N-mass balance model.
1002 Colors and numbers represent boxes found in each of the three zones in terms of
1003 potential productivity (Unit: gC m^{-2} day^{-1}).
1004
1005 Figure 7b. As for 7a, using data from below the pycnocline

Figure 8. Distribution of the three zones during cruises MCH M1-M3 based on salinity data (Lahiry, 2007). Areas shaded in three colors represent the brown, green and blue zones respectively.

Figure 9. Dissolved inorganic nitrogen (DIN) against dissolved inorganic phosphorus (DIP) during sampling periods in the Gulf of Mexico (GOM) and Mid-western Korea (CSK). Nearly all samples had an N:P ratio of < 16, which indicated potential N-limited condition. At a few points near the brown zone the ratio was between 16 -18; this is where light-limitation is expected according to RC02.

List of Tables

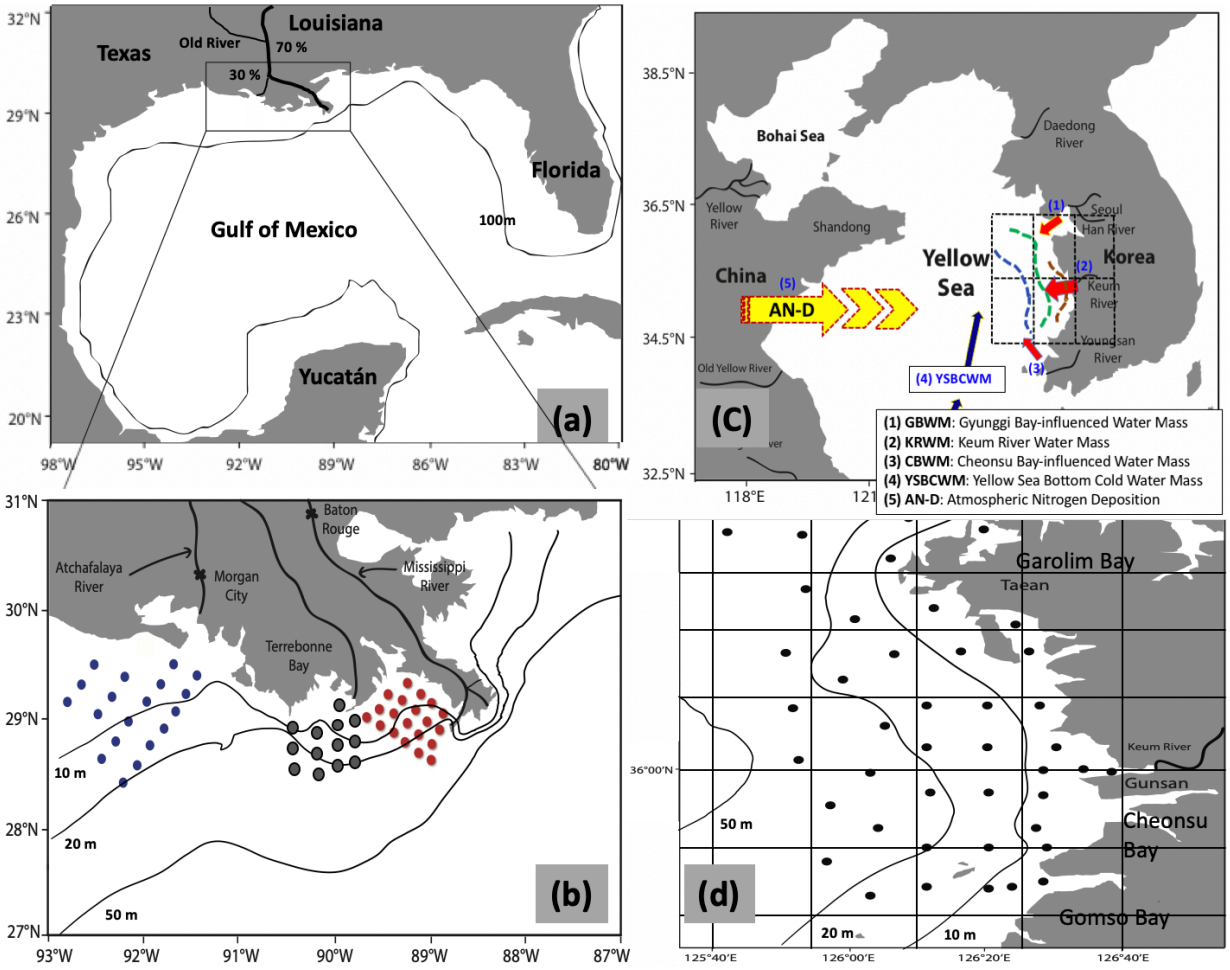

Figure 1. Study sites and sampling areas in the Gulf of Mexico and Korea. (a) shows the sampling area within the northern Gulf of Mexico. Flow in the Mississippi/ Atchafalaya River System is split 30% to the Atchafalaya River, 70% to the Mississippi River. The box is the sampling area. (b) shows station positions from March 2005. Note that MCH project data are widely distributed across the region. Red, grey, and blue stations correspond to sub-regions A (near the Mississippi River), B (between the Mississippi and Atchafalaya), and C (near the Atchafalaya) respectively. (c) shows the sampling area off the west coast of Korea. (d) shows all of the station positions.

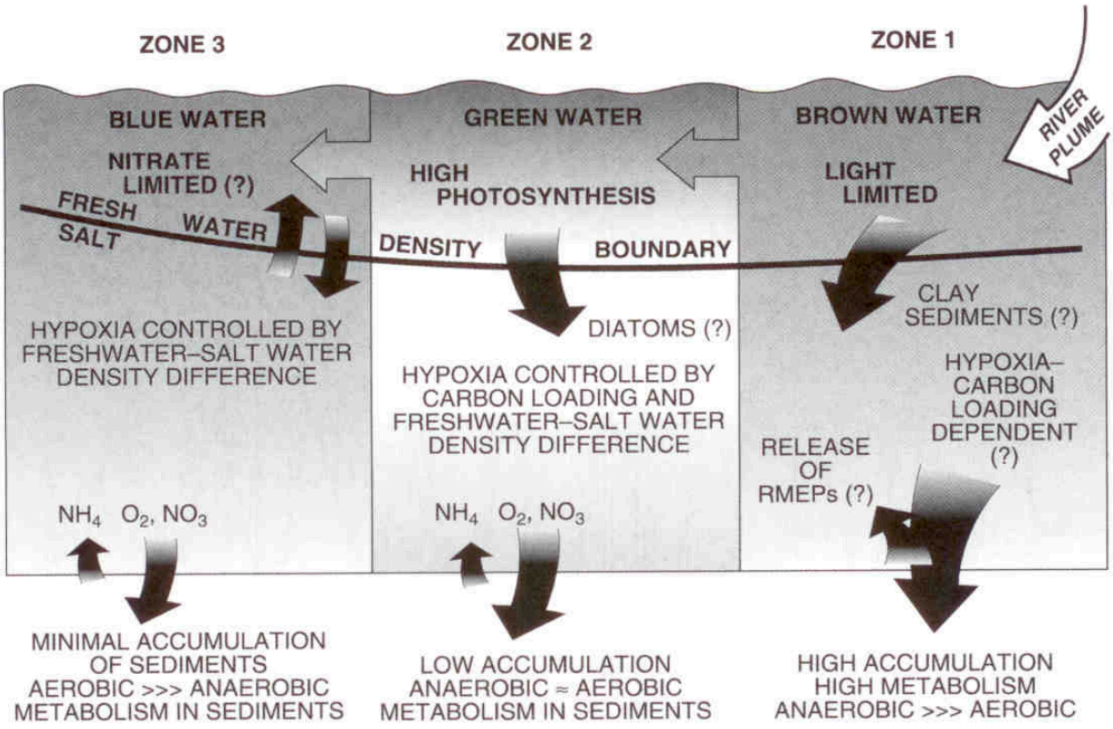

Figure 2. The Rowe and Chapman three zone hypothesis, which describes the physical and biochemical processes that initiate and sustain hypoxia on the Texas-Louisiana Shelf, [Rowe and Chapman, 2002]. RMEPs are Reduced Metabolic End Products. *Reprinted with permission of Gulf of Mexico Science.*

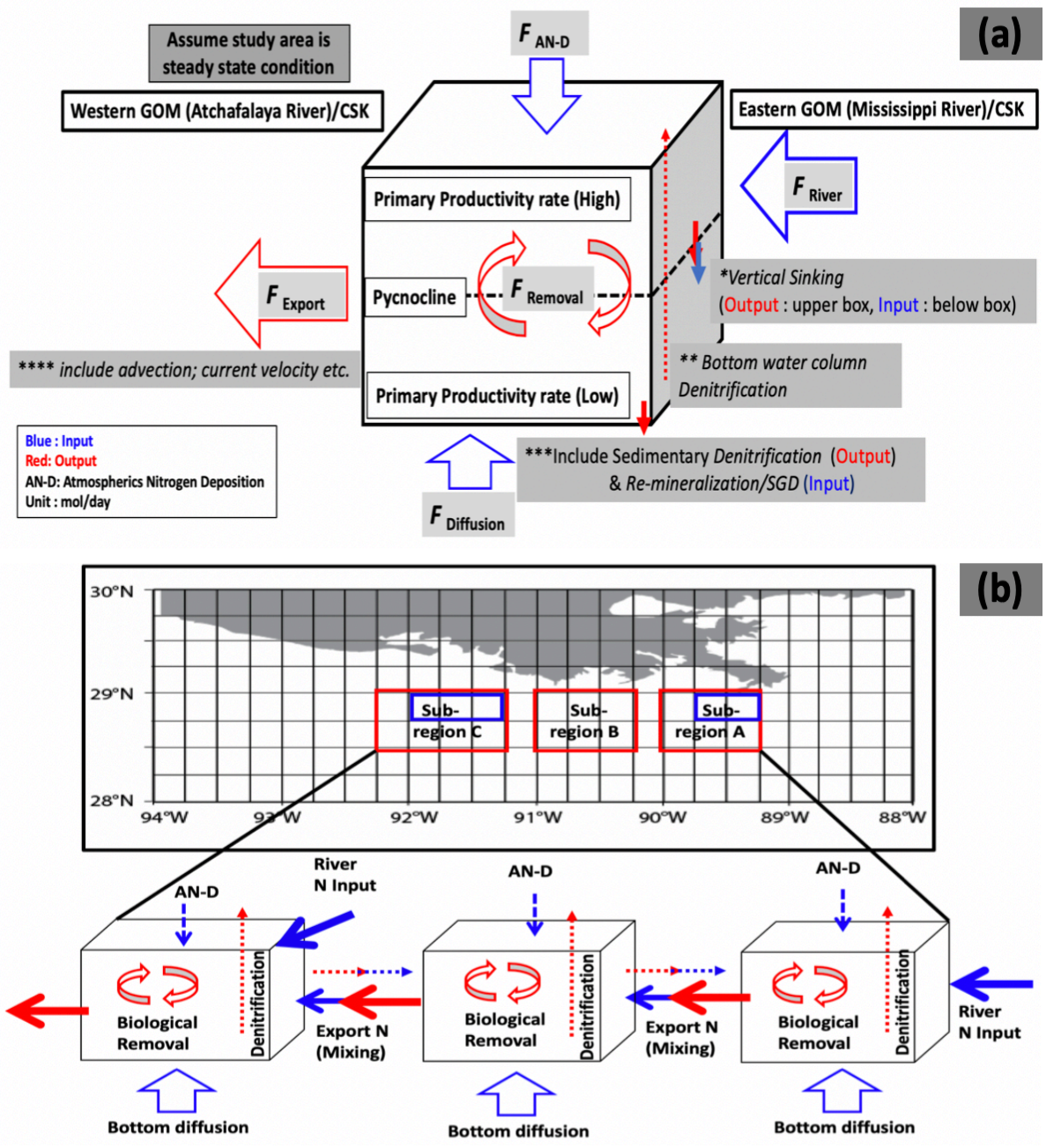

Figure 3. (a) Input (blue) and output (red) sources for each 0.25° box (see text for details); (b) Area of each sub-region (red) and boxes affected by direct riverine input (blue). Export N (Mixing) represents the advective transport term. The processes of biogeochemical and transport processes of both regions are the same and each in/out put factor is the same in the GOM and CSK. Note that transfer between boxes occurs in both directions alongshore and onshore/offshore and is not a one-dimensional process as suggested in the diagram.

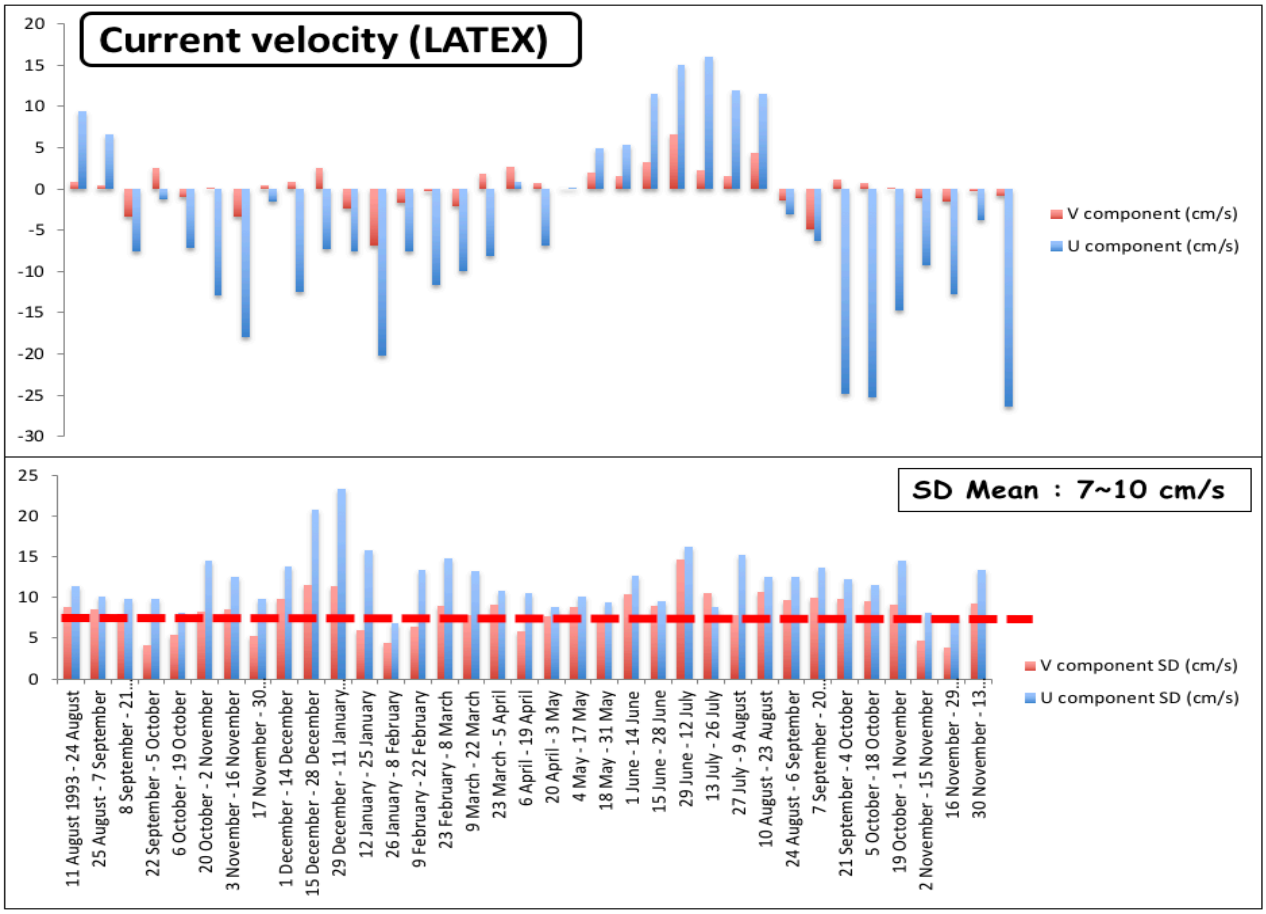

Figure 4. Mean ocean current velocities (a) and standard deviations (b) for biweekly periods from August 1993 through December 1994 based on data from LATEX project. Positive values of U show eastward flow; positive values of V show northward flow.

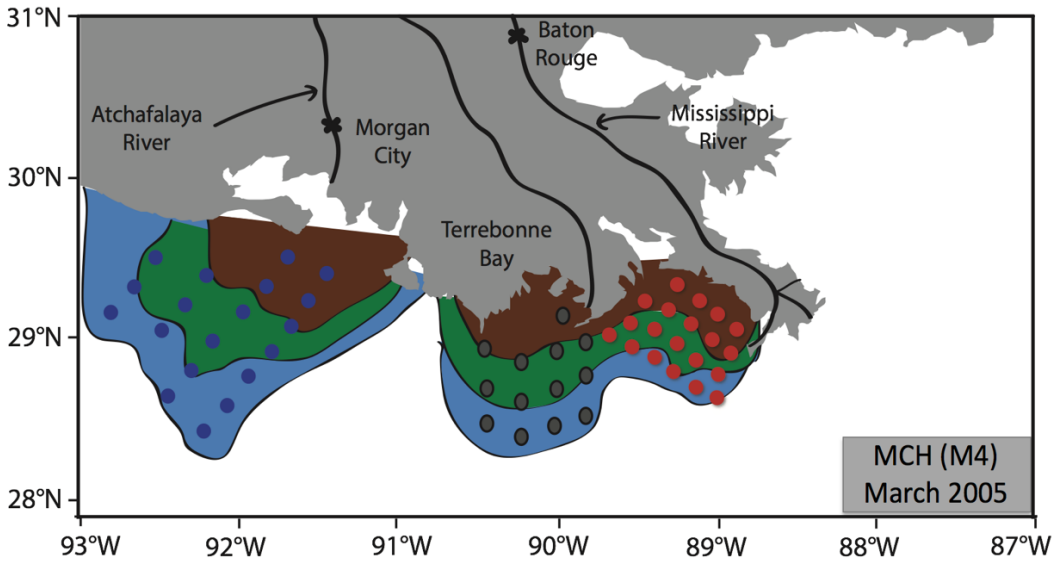

Figure 5. Extent of the three zones defined by RC02 based on the mean concentration of nutrient (DIN) at each station during the MCH M4 cruise in March 2005, showing their correspondence to the three sub-regions used in the box model. Red, grey and blue stations correspond to sub-regions A (near the Mississippi River), B (between the Mississippi and Atchafalaya), and C (near the Atchafalaya) respectively.

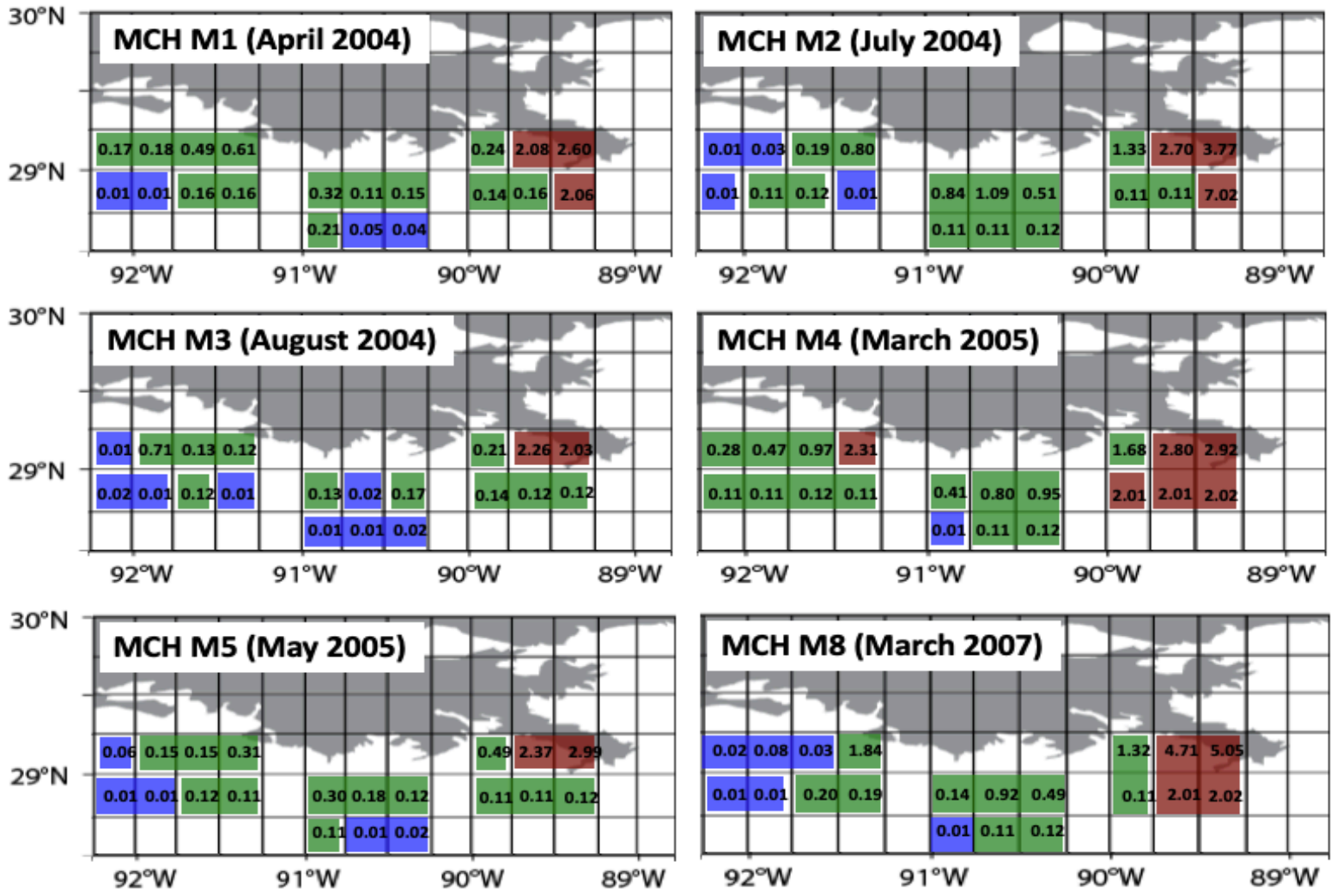

Figure 6a. Areal distributions of the three zones using data from above the pycnocline, based on N-mass balance model results. Colors and numbers represent boxes found in each of the three zones in terms of potential productivity (Unit: gC m^{-2} day^{-1}).

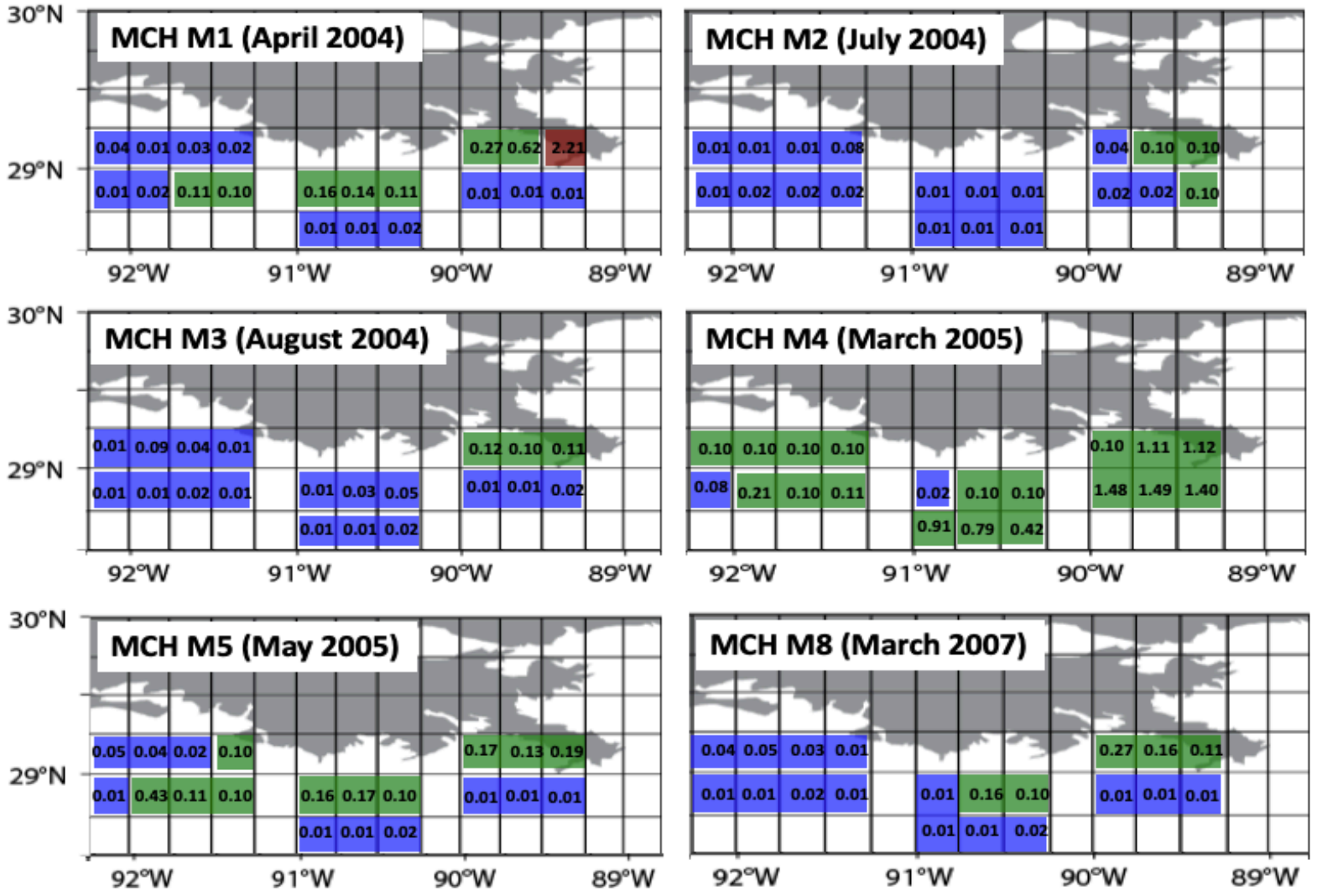

1076

1077 **Figure 6b.** As for 6a, using data from below the pycnocline.

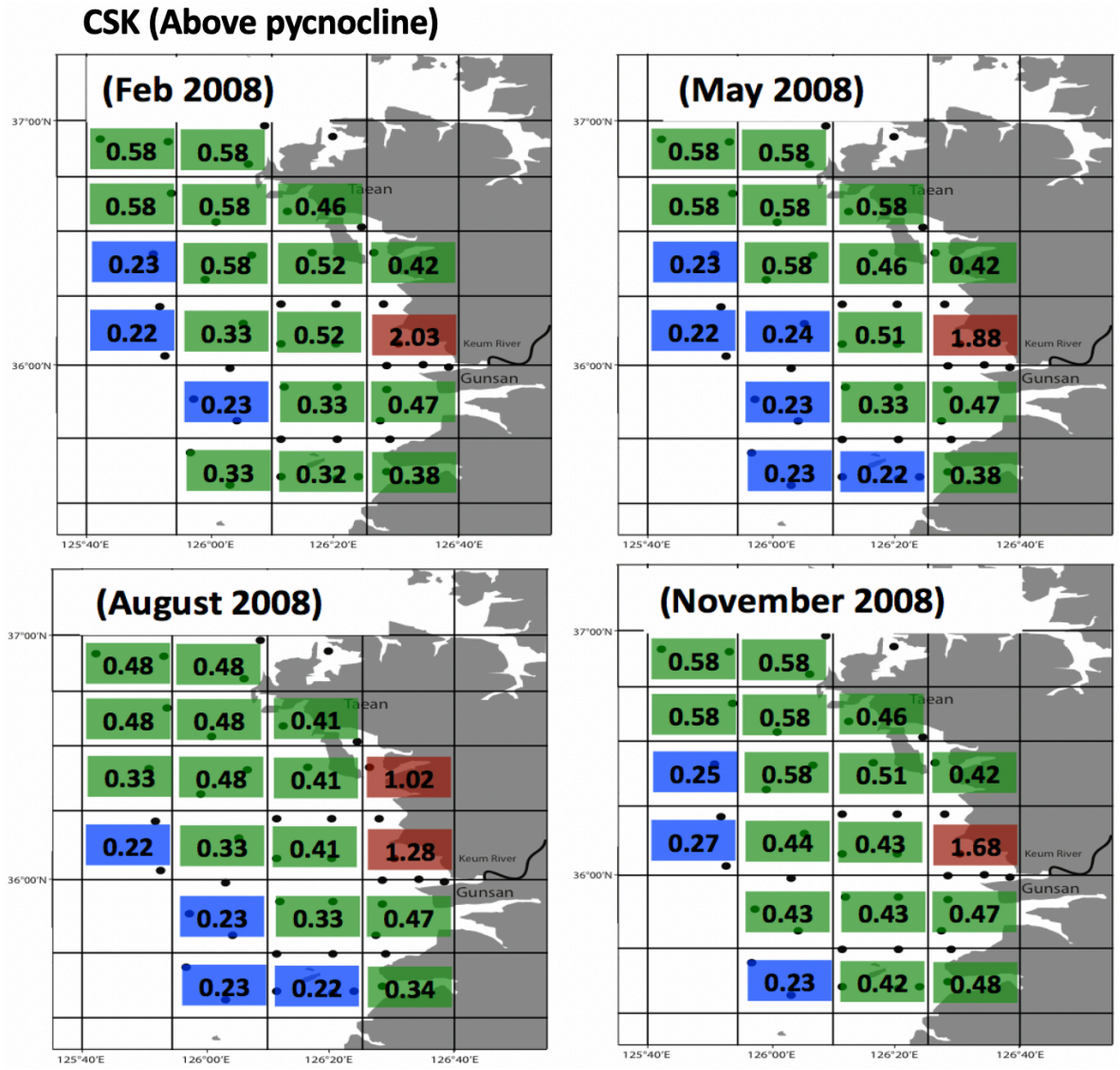

1078

1079 **Figure 7a.** The distribution of the three zones off Mid-western Korea (CSK) above the
1080 pycnocline based on the RC02 hypothesis applied to the N-mass balance model. Colors and
1081 numbers represent boxes found in each of the three zones in terms of potential productivity
1082 (Unit: gC m^{-2} day^{-1}).

1083

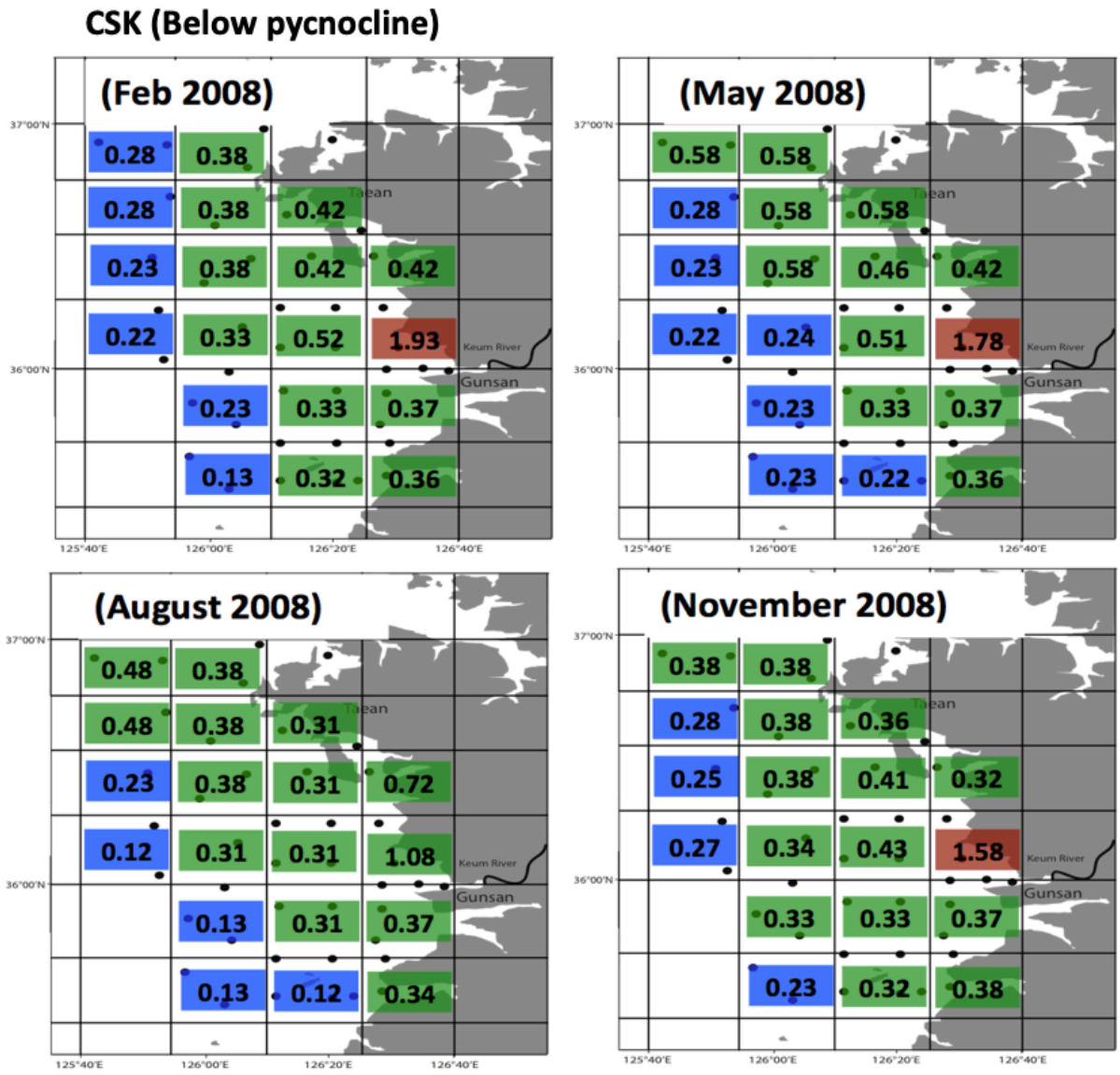

Figure 7b. As for 7a, using data from below the pycnocline.

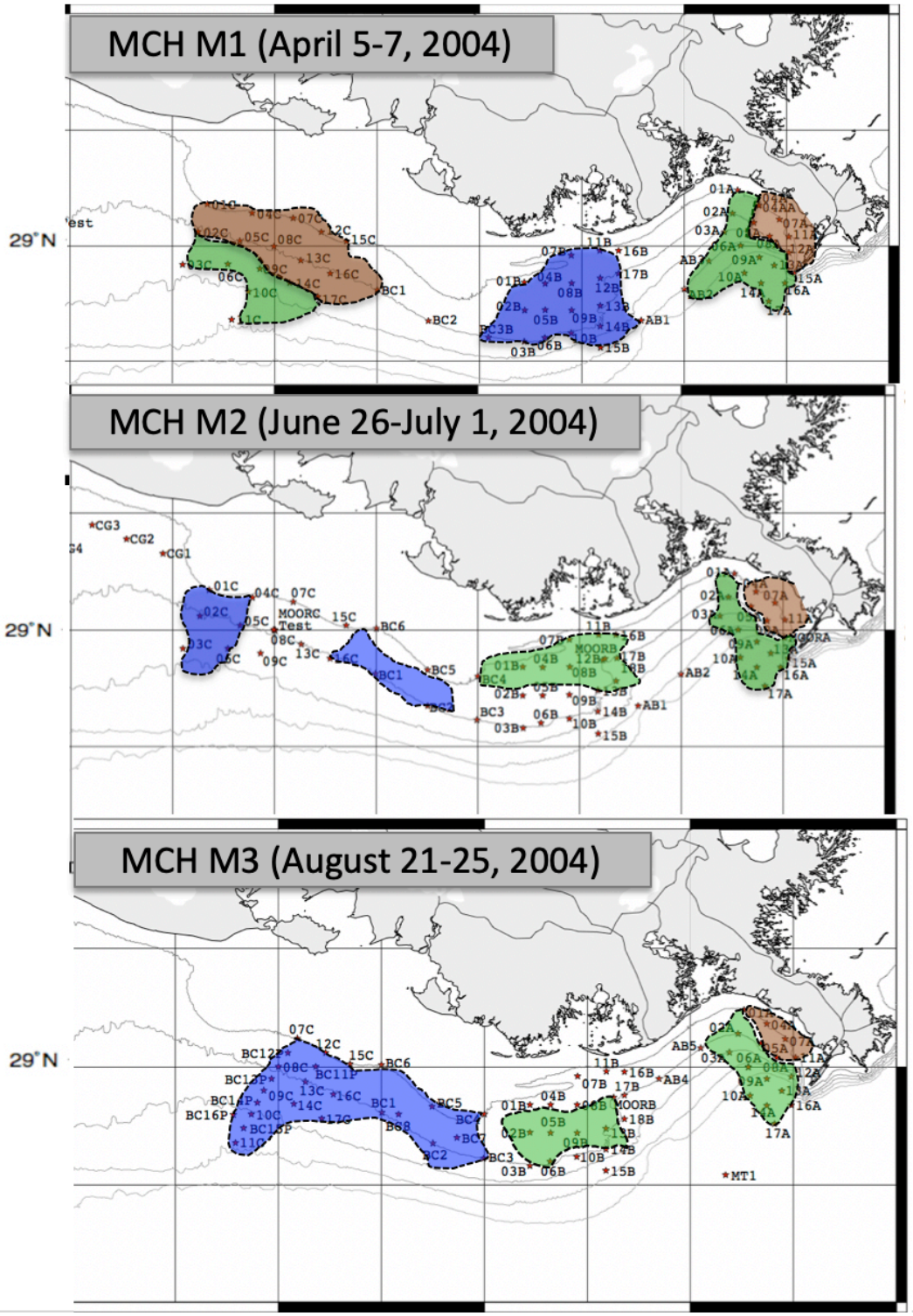

Figure 8. Distribution of the three zones during cruises MCH M1-M3 based on salinity data (Lahiry, 2007). Areas shaded in three colors represent the brown, green and blue zones respectively.

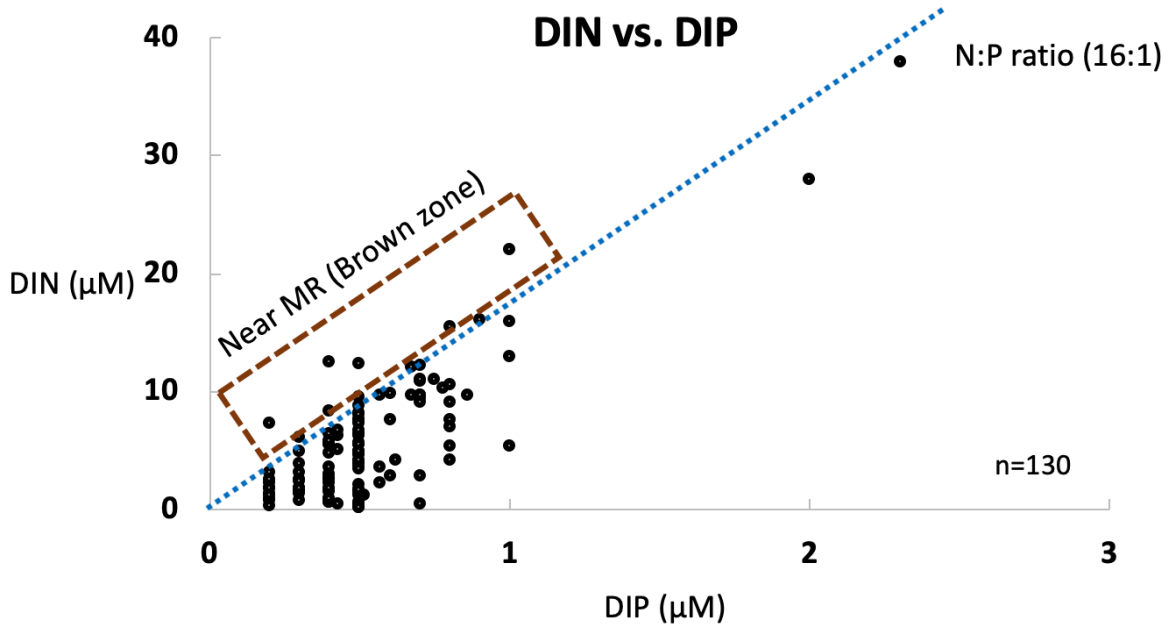

Figure 9. Dissolved inorganic nitrogen (DIN) against dissolved inorganic phosphorus (DIP) during sampling periods in the Gulf of Mexico (GOM) and Mid-western Korea (CSK). Nearly all samples had an N:P ratio of < 16, which indicated potential N-limited condition. At a few points near the brown zone the ratio was between 16 -18; this is where light-limitation is expected according to RC02.

Table 1. Sampling dates for data from Gulf of Mexico projects and the coastal sea of Korea. Winter data are listed for the Gulf of Mexico cruises.

Study area	Date	Cruise number
Gulf of Mexico MCH	5 ~ 7 April 2004	MCH M1
	26 June ~ 1 July 2004	MCH M2
	21 ~ 25 August 2004	MCH M3
	23 ~ 27 March 2005	MCH M4
	20 ~ 26 May 2005	MCH M5
	23 ~ 29 March 2007	MCH M8
Korea CSK	Feb, May, Aug, Nov (2008)	

1103 **Table 2.** Atmospheric Nitrogen Deposition (AN-D) in the USA and in the Yellow Sea.

Watersheds	AN-D (g m^{-2} $year^{-1}$)	References
Casco Bay, ME	0.15	Castro and Driscoll. 2002
Merrimack River, MA	0.12 ~ 0.4	Alexander et al. 2001
Long Island Sound, CT	0.18	Castro and Driscoll. 2002
Delaware Bay, DE	0.22 ~ 0.44	Castro and Driscoll. 2002 Goolsby. 2000
Chesapeake Bay	0.14 ~ 1.74	Alexander et al. 2001 Castro, M. S et al. 2001 Castro and Driscoll. 2002 Goolsby. 2000
Gulf of Mexico	1 ~ 1.15	Wade and Sweet. 2008
Bohai Sea	6.42 ~ 14.25	Shou et al. 2018
Yellow Sea (China on the west side)	1.61 ~ 1.84 2.99 ~ 3.28 3.81 ~ 9.24	Zhao et al. 2015 Luo et al. 2014 Shou et al. 2018
Yellow Sea (Korea on the east side)	1.5 ~ 5.82	Kim (JY) et al. 2010

1104
1105

Table 3. Definitions and values used in N-mass balance model to calculate DIN removal by biological production. (a) Each one quarter degree box; (b) Wade and Sweet 2008 for GOM region; (c) McCarthy et al., 2015 (d) Lee et al., 2012; (e) McCarthy et al., 2015; (f) Qureshi 1995. *F_{Atmo}^{DIN} of CSK region is used as mean values of Asia data in Table 2, which is initially 5 times higher than that of GOM (1.4 X 10^5 mol day^{-1}). ** The unit of F_{Sink}^{DIN} was converted to mol day^{-1} from the unit of original data (gN m^{-2} day^{-1}) with area of box (0.25 m x 0.25 m) and molar mass of N (14 g mol^{-1}). All unit were converted to mol day^{-1} multiplied by area of box (0.25 m x 0.25 m).

Unit	Definitions	Value
A_{Bott} (m^2)	Area of box	6.2 X 10^8 m^2 (a)
C_{Box}^{DIN} (μM)	DIN concentration in each area (box)	
V_S (m^3)	Water volume of box	A_{Bott} X Pycnocline depth
C_{EX}^{DIN} (mmol m^{-3})	Different concentration between each box **C_{EX}= (C_{On} - C_{Off}) or (C_{East} – C_{West}) for DIN**	
λ_{Mix} (day^{-1})	Mixing rate of each box to box (**A reciprocal of the water residence time**)	
F_{River} (day^{-1})	River discharge	
F_{River}^{DIN} (mol day^{-1})	DIN flux from each river discharge	
F_{Atmo}^{DIN} (mol day^{-1})	Diffusive flux from Atmospheric deposition (Bulk N deposition rate x A_{Bott} ($A_{surface\ of\ ocean}$) for DIN	1.4 X 10^5 mol day^{-1} * (b)
F_{Bott}^{DIN} (mol day^{-1})	Benthic flux from the bottom sediments (Net DIN release considered regeneration, groundwater inputs, and uptake of NO_2/ NO_3)	1.2 mmol N m^{-2} day^{-1} (c) 6.2 mmol N m^{-2} day^{-1} (d)
F_{Export}^{DIN} (mol day^{-1})	An advection term which calculated from the current velocity	
F_{Deni}^{DIN} (mol day^{-1})	Denitrification in the water column	2.1 mmol N m^{-2} day^{-1} (e)
F_{Sink}^{DIN} (mol day^{-1})	Vertical sinking of DIN flux from sediment trap data	0.1 ~ 1 gN m^{-2} day^{-1} ** (f)
$F_{Removal}^{DIN}$ (day^{-1})	Removal by biological production (Assuming that the other removal factors are negligible above the pycnocline layer)	

Table 4. Simulation results for selected model scenarios based on MCH M1 (5 ~ 7 April 2004). Biological production is calculated by our N-mass balance model. Oxygen demand is calculated by Redfield stoichiometry ratio (C: $-O_2$ = 106: 138) (Unit: gC m^{-2} day^{-1}).

	F_{River}	$F_{AN\text{-}D}$	$F_{Bott/SGD}$	**Biological production**	**Oxygen demand**
Nominal Value	1.4×10^7 (~98 %)	1.4×10^5 (~1 %)	1.4×10^5 (~1 %)	Base line	
Scenario 1	5.6×10^6 (~93 %)	2.8×10^5 (~5%)	1.4×10^5 (~2%)	~45% decreased	~58% decreased
Scenario 2	9.8×10^6 (~96 %)	2.8×10^5 (~3%)	1.4×10^5 (~1%)	~22% decreased	~28% decreased
Scenario 3	1.7×10^7 (~97 %)	2.8×10^5 (~2%)	1.4×10^5 (~1%)	~17% increased	~21% increased

Table 5. Simulation results for selected model scenarios based on CSK (February 2008) data. Biological production is calculated by our N-mass balance model. Oxygen demand is calculated by the Redfield stoichiometry ratio (C: $-O_2$ = 106: 138) (Unit: gC m^{-2} day^{-1}).

	F_{River}	$F_{AN\text{-}D}$	$F_{Bott/SGD}$	**Biological production**	**Oxygen demand**
Nominal Value	1.9×10^6 (~60%)	6.0×10^5 (~20%)	6.0×10^5 (~20%)	Base line	
Scenario 1	7.2×10^5 (~29%)	1.2×10^6 (~47%)	6.0×10^5 (~24%)	~13% decreased	~16% decreased
Scenario 2	1.3×10^6 (~41%)	1.2×10^6 (~39%)	6.0×10^5 (~20%)	~2% decreased	~2% decreased
Scenario 3	2.2×10^6 (~55%)	1.2×10^6 (~30%)	6.0×10^5 (~15%)	~25% increased	~32% increased